frontiers | Frontiers in Batteries and Electrochemistry

TYPE Review
PUBLISHED 17 January 2024
DOI 10.3389/fbael.2023.1268412

OPEN ACCESS

EDITED BY
Moran Balaish,
Technical University of Munich, Germany

REVIEWED BY
Uk Sim,
Korea Institute of Energy Technology (KENTECH), Republic of Korea
Wenli Zhang,
Guangdong University of Technology, China

*CORRESPONDENCE
Drandreb Earl O. Juanico,
reb.juanico@tip.edu.ph

RECEIVED 28 July 2023
ACCEPTED 27 December 2023
PUBLISHED 17 January 2024

CITATION
Juanico DEO (2024), Revitalizing lead-acid battery technology: a comprehensive review on material and operation-based interventions with a novel sound-assisted charging method. *Front. Batteries Electrochem.* 2:1268412. doi: 10.3389/fbael.2023.1268412

Revitalizing lead-acid battery technology: a comprehensive review on material and operation-based interventions with a novel sound-assisted charging method

Drandreb Earl O. Juanico[1,2]*

[1]Advanced Batteries Center Philippines, Quezon City, Philippines, [2]Technological Institute of the Philippines, Quezon City, Philippines

This comprehensive review examines the enduring relevance and technological advancements in lead-acid battery (LAB) systems despite competition from lithium-ion batteries. LABs, characterized by their extensive commercial application since the 19th century, boast a high recycling rate. They are commonly used in large-scale energy storage and as backup sources in various applications. This study delves into the primary challenges facing LABs, notably their short cycle life, and the mechanisms underlying capacity decline, such as sulfation, grid corrosion, and positive active material (PAM) degradation. We present an in-depth analysis of various material-based interventions, including active material expanders, grid alloying, and electrolyte additives, designed to mitigate these aging mechanisms. These interventions include using barium sulfate and carbon additives to reduce sulfation, implementing lead-calcium-tin alloys for grid stability, and incorporating boric and phosphoric acids in electrolytes for enhanced performance. In contrast, operation-based strategies focus on optimizing battery management during operation. These include modifying charging algorithms, employing desulfation techniques, and integrating novel approaches such as reflex and electroacoustic charging. The latter, a promising technique, involves using sound waves to enhance the electrochemical processes and potentially prolong the cycle life of LABs. Initial findings suggest that electroacoustic charging could revitalize interest in LAB technology, offering a sustainable and economically viable option for renewable energy storage. The review evaluates the techno-economic implications of improved LAB cycle life, particularly in renewable energy storage. It underscores the potential of extending LAB cycle life through material and operation-based strategies, including the innovative application of electroacoustic charging, to enhance the competitiveness of LABs in the evolving energy storage market.

KEYWORDS

lead acid batteries, cycle life, electroacoustic charging, levelized cost of storage, renewable energy storage

1 Introduction

The lead-acid battery (LAB) system is a mature technology with a broad scope of commercial applications that has existed since the 19th century. It is currently deployed in both large-scale, such as energy storage modules for power grids, as well as in small-scale applications, such as backup sources in uninterrupted power supplies and engine starters for both hybrid electric and internal combustion-engine vehicles, to name a few (Rydh, 1999; Matteson and Williams, 2015; Rand and Moseley, 2015; Yang et al., 2017; Kim et al., 2018; Lopes and Stamenkovic, 2020; Kebede et al., 2021). Moreover, the recycling rate of used LAB units can be as high as 99%, making it the only rechargeable battery technology that is close to a circular economy (Lopes and Stamenkovic, 2020; Zhang et al., 2022). Although mature, LAB technology has been considered a "dead end" in product development, disincentivizing further scientific inquiry. Also, portability and lead toxicity issues contributed to the push away from LAB systems, motivating the quest for alternative chemistries that eventually catapulted the broad acceptance of the lithium-ion battery (LiB) as a versatile technology in today's mobility-dominated economy. Notwithstanding these advances in LiB and emerging rechargeable battery chemistries, the LAB system retains its lion's share of the market. This status is primarily due to the abundant and inexpensive raw materials and ease of manufacturing and recycling of LAB systems.

The main setback of the LAB system is its short cycle life. On average, LAB units are replaced every 3–6 years (or about 150–200 cycles for a 100 Ah LAB cycled at 100% depth of discharge (Hutchinson, 2004)), and the short-term usages prompt frequent replacements that incur additional operation costs. The brief cycle life primarily results from the capacity decline due to the combined effects of different damage and aging mechanisms affecting the essential LAB components (i.e., positive and negative electrodes, current collector, and electrolyte). These deterioration mechanisms include irreversible sulfation, positive grid corrosion, positive active material (PAM) degradation, dehydration, thermal runaway, electrolyte stratification, internal short circuits, and mechanical damages (Catherino et al., 2004; Ruetschi, 2004; Kelly and Galgana, 2009; Shi et al., 2013; Yang et al., 2017). Among these mechanisms, hard or irreversible sulfation, PAM degradation, and positive grid corrosion were identified as primary failure modes (Yang et al., 2017). Most of the listed problems are related to or contribute to the cause of one or more of the identified failure mechanisms (Guo et al., 2007; Shi et al., 2013; Gandhi, 2020).

This work presents a comprehensive review of various techniques utilized to address the abbreviated cycle life of the lead acid system, coupled with insights into the potential application of electroacoustic charging to prolong cycle life. Electroacoustic charging falls under operation-based methods devised to intervene in the cell's natural progression towards its end of life.

The review begins by delving into the intricacies of the LAB operation, specifically, the charge-discharge process and its correlation with failure modes and related aging mechanisms. In subsequent discussions, attention is directed towards the diverse array of methods devised to mitigate the effects of aging, thereby extending cycle life. These interventions are bifurcated into two principal categories: material-based and operation-based approaches.

Material-based methodologies are targeted techniques principally designed to tackle specific aging mechanisms through chemical or electrochemical means, often involving modification of the cell components' composition. Usually performed offline, these techniques frequently address multiple aging mechanisms concurrently, employing tools such as active material expanders and electrolyte additives (Bullock, 1979; Shiomi et al., 1997; Vermesan et al., 2004; Vanýsek et al., 2020; Wu et al., 2020).

On the flip side, operation-based strategies employ a blend of electrochemistry and electromechanical engineering to address a single issue and simultaneously counteract multiple aging mechanisms. As their name suggests, these strategies are conducted during battery operation and include varied charging strategies aimed at desulfation and capacity restoration, as well as passive maintenance for optimal charge-discharge operation (Shi et al., 2013; Mizumoto et al., 2018; Lavety et al., 2020; Singh et al., 2021; Tao et al., 2021). The discussion will focus on the significant advancements in LAB technology while addressing the inherent challenges and limitations of these approaches.

Under the banner of operation-based approaches, the discussion explores the emerging literature on a novel ultrasound-based technique for extending cycle life. Initially noted for enhancing the cycle life of lithium-metal (Li-metal) batteries, proponents suggest this method maintains a chemistry-agnostic disposition, showing promise for incorporation into other battery chemistries utilizing liquid electrolytes (Huang et al., 2020). Preliminary evidence from ongoing research offers a proof of concept regarding this technique's potential to ameliorate the LAB systems' cycle life performance. Such exploration might invigorate interest in LAB technology, fostering renewed research vigor in this established domain. The discourse will weigh the repercussions of extended LAB cycle life through succinct economic feasibility analysis, spotlighting the levelized cost of storage and profitability metrics. The examination will critique the present status of LABs in renewable energy storage applications, contrasting it with the standing of LiBs, currently the favored battery technology for renewable energy integration.

A significant focus of this review is the potential application of electroacoustic charging in extending the cycle life of LABs. Initially studied in lithium-metal batteries, this novel approach employs sound waves to influence electrochemical processes, showing promise in enhancing LAB efficiency. The review discusses the economic implications of these technological advancements, particularly in renewable energy storage, where extended battery life could significantly impact energy systems' economic feasibility and environmental sustainability.

2 LAB charge-discharge process and failure modes

2.1 Sulfation mechanisms

Irreversible sulfation is frequently implicated in battery failure, wherein lead sulfate ($PbSO_4$) irreversibly accumulates on the

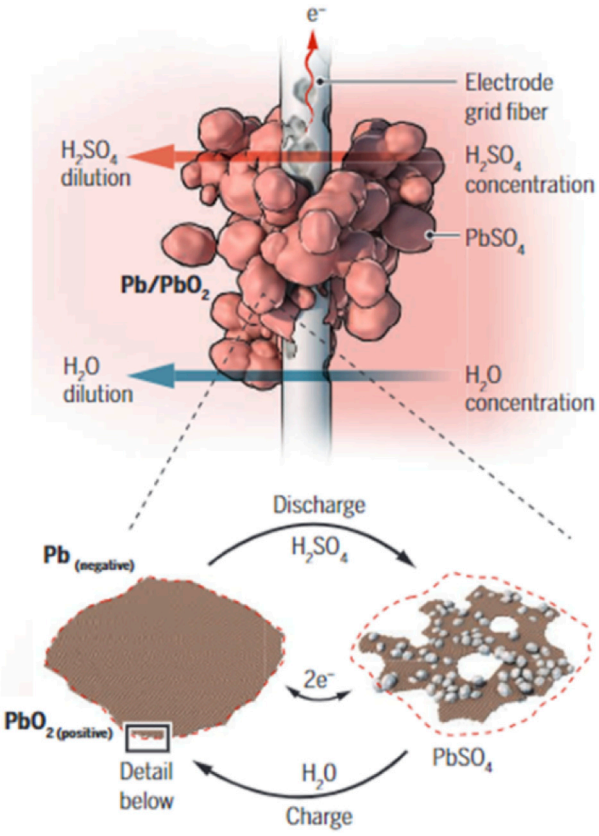

FIGURE 1
Depiction of the charge-discharge cycle in a lead-acid battery, illustrating the material alterations concurrent with electrochemical reactions on an electrode grid fiber's surface (Lopes and Stamenkovic, 2020).

electrodes. Given its detrimental impacts on battery longevity, the issue of sulfation has naturally been the subject of numerous investigations. This section delves into the underpinning mechanisms and contributory factors leading to this undesirable phenomenon, with a comprehensive examination of the half-cell and overall reactions, as denoted in Eq. s 1–3 (Archdale and Harrison, 1972; Weininger, 1974; Pavlov, 2011). Unraveling these underlying processes intends to illuminate potential strategies and interventions to prevent premature battery failure resulting from irreversible sulfation. A holistic understanding of these principles could thus pave the way towards more resilient and long-lasting battery systems.

Negative electrode:

$$Pb + SO_4^{2-} \leftrightarrow PbSO_4 + 2e^- \quad (1)$$

Positive electrode:

$$PbO_2 + 4H^+ + SO_4^{2-} + 2e^- \leftrightarrow PbSO_4 + 2H_2O \quad (2)$$

Overall reaction:

$$Pb + PbO_2 + 2H_2SO_4 \leftrightarrow 2PbSO_4 + 2H_2O \quad (3)$$

During discharge, an oxidation process is observed to affect lead (Pb), or the negative active material (NAM), while lead dioxide (PbO_2), or the positive active material (PAM), undergoes a corresponding reduction process. The electrochemical dissolution of these active materials gives rise to Pb^{2+} ions. In the battery's environment, these ions readily interact with free SO_4^{2-} anions to form $PbSO_4$ crystals, which precipitate onto the surfaces of the electrodes. Concurrently, the discharge reaction occurring at the PAM generates water, leading to the dilution of the electrolyte (Takehara, 2000; Pavlov et al., 2004). These interlinked processes, central to the operation of lead-acid batteries, are depicted in Figure 1. Illustrating these complex reactions aims to furnish deeper insight into the operation of the LAB system and the associated emergent challenges.

The charge-discharge process within the lead-acid cell, characterized by dissolution-precipitation, forms $PbSO_4$ crystals within the active material. Von Weimarn's rule suggests that the size of $PbSO_4$ crystals increases as the initial Pb^{2+} supersaturation decreases. Experiments on PbO_2 and Pb electrodes show the influential role of acid concentration in modulating Pb^{2+} supersaturation, as demonstrated in Figure 2 (left) (Takehara and Kanamura, 1984; Baird et al., 1999). High Pb^{2+} supersaturation leads to faster nucleation than growth, producing tiny $PbSO_4$ crystals, while the opposite occurs at low Pb^{2+} supersaturation, generating large $PbSO_4$ crystals, as displayed in Figure 2 (right) (Kanamura and Takehara, 1992).

$PbSO_4$ nucleation can also transpire in non-polarized environments. Research shows spontaneous $PbSO_4$ nucleation on an initially polarized Pb electrode upon switching the electrode potential to an open circuit due to a favorable corrosion mechanism at low pH (Knehr et al., 2014). A chemical-recrystallization model describes $PbSO_4$ crystals forming during the dissolution-precipitation step, then recrystallizing via Ostwald ripening as Pb^{2+} ions release into the electrolyte (Yamaguchi et al., 2000). This recrystallization accounts for why discharged cells left idle risk irreversible sulfation. Additionally, large $PbSO_4$ crystals form on the PAM surface after extended low C-rate discharge (Jin et al., 2017).

The dissolution-precipitation mechanism is also applicable during charging. $PbSO_4$ crystals on the electrodes dissolve in diluted H_2SO_4, releasing Pb^{2+} ions, which then migrate into the active sites within the electrodes. Subsequently, a charge transfer process ensues, reforming Pb on the negative electrode and Pb^{4+} on the positive electrode (Pavlov et al., 2004; Pavlov, 2011). However, despite the theoretical reversibility of charge-discharge reactions in the lead-acid cell, several studies have reported incomplete reconversion of $PbSO_4$ during charging (Takehara and Kanamura, 1984; Takehara, 2000; Pavlov et al., 2004; Yang et al., 2017; Broda and Inzelt, 2020). This results in residual $PbSO_4$ accumulation, driving irreversible sulfation.

The inherent properties of $PbSO_4$, an ionic crystal with poor solubility and electronic conductivity, contribute to the inefficiencies of the charging process. Few Pb^{2+} ions are generated, which hampers charge and mass transfer—additionally, charging in aqueous electrolytes results in gassing reactions, which consume the charge intended for the recovery of active materials. Consequently, a portion of the $PbSO_4$ deposit remains unreacted despite sufficient charge (Takehara, 2000; Gandhi, 2020). For charging to be efficient, a large flux of Pb^{2+} ions is needed to maintain a high reaction rate, and these ions must reach the active sites within the electrode bulk for charge transfer to proceed.

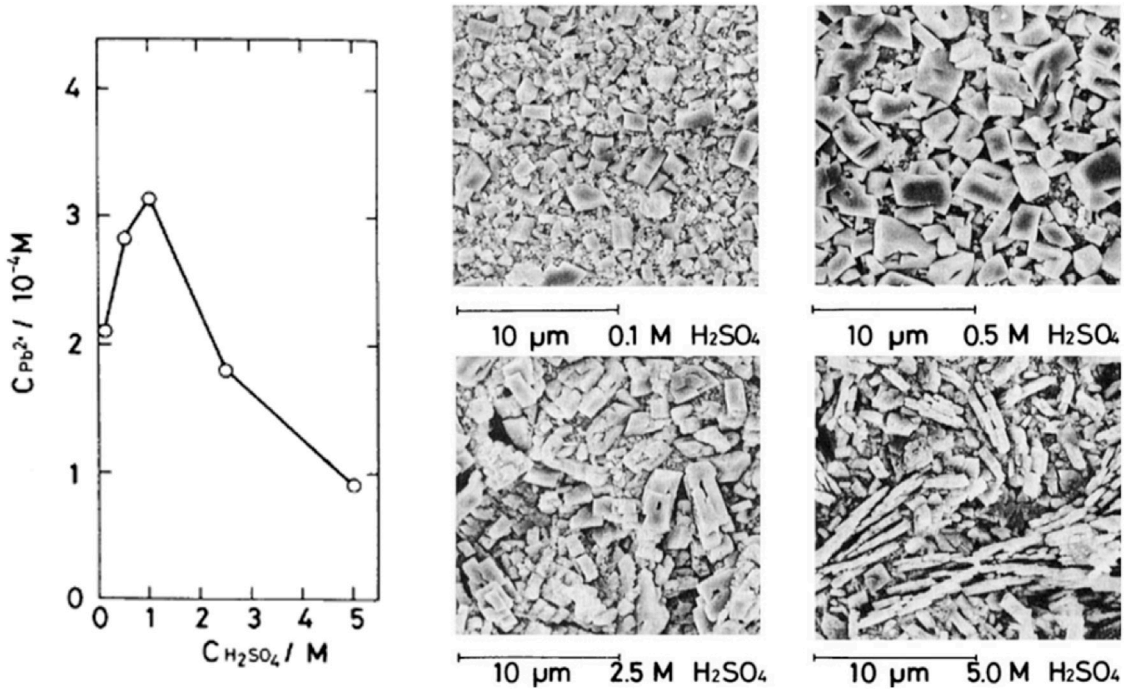

FIGURE 2
Influence of Pb^{2+} supersaturation on the $PbSO_4$ crystal size. The H_2SO_4 concentration affects Pb^{2+} supersaturation (left). Scanning electron micrographs showcase the electrode surface post-discharge of PbO_2 at 2.5 mA/cm^2 under varying H_2SO_4 concentrations (Takehara, 2000).

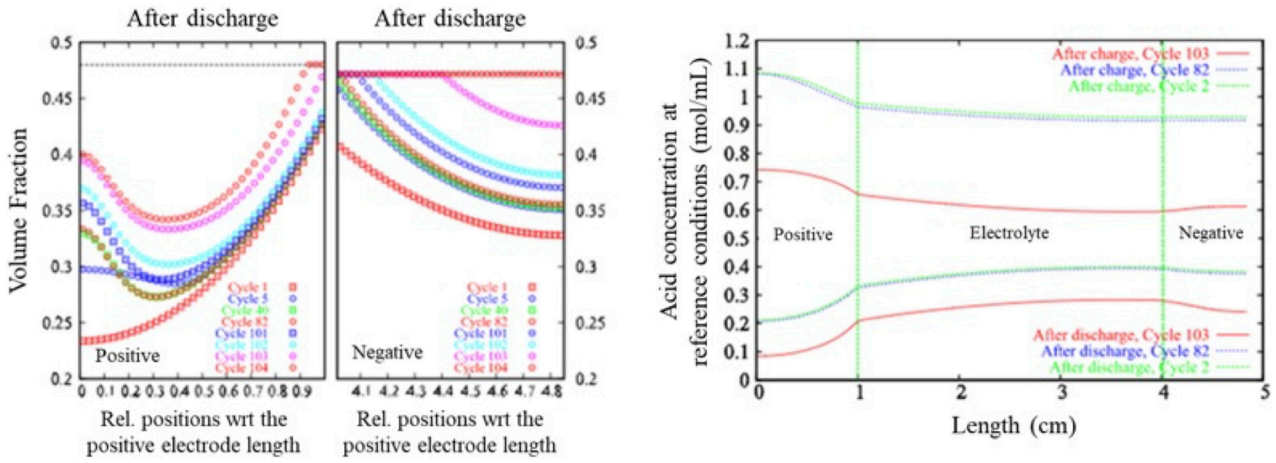

FIGURE 3
Variation of $PbSO_4$ volume fraction with respect to position at discharge termination. The dotted line at the top (left) illustrates the volume fraction at critical conversion. Acid concentration's spatial profile at the culmination of 2nd, 82nd, and 103rd cycles. The upper three curves represent the charging phase, while the lower three signify the discharge phase (right) (Guo et al., 2007).

In lead-acid cells, sulfation and utilization of active materials differ between positive and negative electrodes, as demonstrated by higher $PbSO_4$ volume and uneven reaction rates in the negative electrode (Gandhi, 2020) (Figure 3). Electrolyte concentration discrepancies are observed near the electrodes post-charge and discharge (Gandhi, 2020). An *in-operando* study revealed a higher concentration gradient and reaction rate near the positive electrode (Takamatsu et al., 2020). Differing sulfation behavior and unique bilayer film compositions in both electrodes further complexify the system (D alkaine et al., 2009). Despite thermodynamic concerns, PbO's presence in H_2SO_4 has been proposed (Pavlov, 2011). Electrolyte stratification leads to sulfation variance across the cell's vertical profile, with prominent stratification during charging (Takamatsu et al., 2020). Two stratification-induced sulfation mechanisms have been introduced (Guo et al., 2007), as well as disparities in hydrogen and oxygen

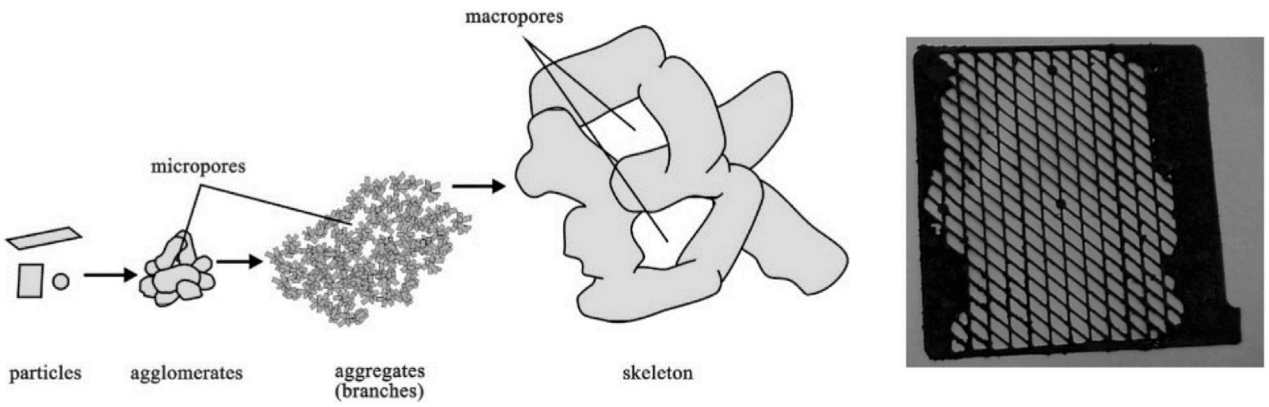

FIGURE 4
Fundamental structural components of the positive active mass (left) (Dimitrov and Pavlov, 2001). Illustration of a positive electrode featuring a deteriorated PAM structure (right) (Ruetschi, 2004).

evolution during charging (Pavlov and Pashmakova, 1987; Zhang et al., 2010; Gandhi, 2020). Understanding these complexities is vital for the advancement of lead-acid battery technology.

2.2 PAM degradation

The negative lead electrode's propensity for irreversible sulfation, a fundamental failure mode, has been well-established in previous sections (Pavlov et al., 2004; Zhang et al., 2010; Spanos et al., 2016). However, the positive electrode also undergoes a failure process, leading to premature capacity loss, a broad term encompassing the physicochemical phenomena leading to degradation, softening, shedding, or sludging of the PAM, or issues with the metallic grid (Ruetschi, 2004; Jin et al., 2017; Yang et al., 2017; Zhang et al., 2017; Hossain et al., 2020).

The fundamental PAM structure, illustrated in Figure 4 (left), is composed of PbO_2 particles that coalesce into agglomerates, forming micro-porous branches, which link together to create the macro-porous PAM skeleton (Pavlov et al., 1989; Dimitrov and Pavlov, 2001; Ruetschi, 2004; Yang et al., 2017). With progressive battery cycling, the PAM structure experiences degradation and eventual collapse due to the stress acquired from extensive volume changes of the active mass (Pavlov and Bashtavelova, 1986; Yang et al., 2017).

Studies by Pavlov and Bashtavelova have documented a decrease in the apparent density of various PAM samples following battery cycling, attributed to an increase in total pore volume (Pavlov and Bashtavelova, 1986; Yang et al., 2017). Similarly, Chang reported significant structural changes in the PAM from its as-cured state to its failed state, noting the considerable reduction in the density of PAM, from 9.81 g/cm^3 post-formation stage to 6.75 g/cm^3 upon cell failure after 126 cycles (Chang, 1984).

Critical to the PAM structure are different PbO_2 phases, with α-PbO_2 aggregates providing mechanical support and β-PbO_2 crystallites serving as the capacity carrier. While α-PbO_2 is less involved in cycling due to its poor electrochemical activity, β-PbO_2, although prone to shedding, is vital for carrying capacity (Pavlov and Bashtavelova, 1986; Pavlov et al., 1989; Egan et al., 2011; Yang et al., 2017). Ball et al.'s research on the proportions of α-PbO_2 and β-PbO_2 in PAM samples from spent LAB units underpins the importance of this balance (Bullock and Tiedemann, 1980; Ball et al., 2002a).

Pavlov et al. have also determined that maintaining an H_2SO_4 concentration above 1.5 M (1.095 s.g.) during discharge is crucial to preventing excessive PAM shedding (Pavlov, 1992; Pavlov et al., 2004). This research contributes to a deeper understanding of PAM behavior under operational conditions, elucidating the importance of physicochemical properties in determining the life cycle and reliability of lead-acid batteries.

Lead-acid battery PAM, composed of PbO_2 in crystalline or gel form, creates an interconnected micro-porous structure (Pavlov et al., 1989; Dimitrov and Pavlov, 2001; Ruetschi, 2004; Yang et al., 2017) (Figure 4). Degradation occurs as the structure collapses under volume changes, notably reducing PAM density and increasing pore volume (Pavlov and Bashtavelova, 1986; Pavlov et al., 1989; Dimitrov and Pavlov, 2001; Ruetschi, 2004; Yang et al., 2017). Chang's study describes the PAM structure's weakening, with prominent pores (size scales >50 μm) increasing in numbers (Chang, 1984). PAM comprises different PbO_2 phases, each contributing to its mechanical stability and capacity (Pavlov and Bashtavelova, 1986; Pavlov et al., 1989; Egan et al., 2011; Yang et al., 2017). Changes in the proportions of α-PbO_2 and β-PbO_2 phases depend on the cell's state and the acidity during charging, affecting crystal formation and redox processes. Understanding these complexities aids in enhancing lead-acid battery efficiency and durability.

2.3 Positive grid corrosion

LAB failure, particularly at the positive electrode, can also be associated with excessive grid corrosion. The electrode's metallic grid, a composition of Pb and alloying elements, is crucial for the positive plate's electron conduction and mechanical stability. However, corrosion is an anticipated phenomenon, given the grid's acidic environment (Catherino et al., 2004; Ruetschi, 2004; Yang et al., 2017). An image of a deteriorated positive grid caused by extensive corrosion is depicted in Figure 5 (left). In this case,

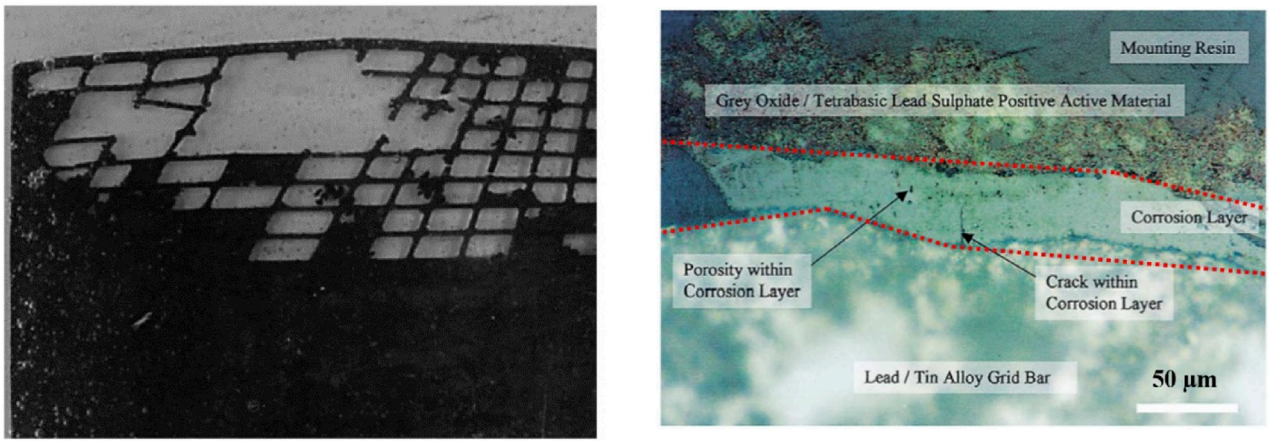

FIGURE 5
Degraded positive grid of a starter lead-acid battery (LAB) (left) (Ruetschi, 2004). Micrographic cross-sectional view of a buffed positive electrode, with the corrosion layer demarcated by red dashed lines (right) (Ball et al., 2002b).

corrosion consumes the metal, causing the collapse of the active mass–a condition that leads to irreversible battery failure (Catherino et al., 2004; Ruetschi, 2004; Yang et al., 2017).

An intriguing aspect of this corrosion process is the formation of a protective layer during battery cycling, which serves to passivate the grid surface, thereby curbing the corrosion rate. Figure 5 (right) illustrates a typical corrosion layer at the interface between the PAM and the metallic grid (Ball et al., 2002b; Ruetschi, 2004; Yang et al., 2017). The corrosion layer's inception commences during the curing stage of active materials, subsequently thickening as the battery continues to cycle.

The fundamental corrosion reaction typically transforms the metallic Pb within the grid into PbO_2 (Eqs. 4–6). The corrosion layer, composed of PbO and PbO_2, significantly impacts the LAB's efficiency and longevity. This layer, which thickens in cells undergoing numerous cycles or overcharging, hinders electron flow from the PAM to the grid, diminishing battery capacity. This effect is pronounced in reduced-capacity cells, where quicker charging accelerates corrosion layer growth (Ball et al., 2002a). Unrestrained, the corrosion process can progressively consume the grid, leading to a condition known as grid corrosion failure. Here, the grid's cross-sectional area shrinks to the point where it can no longer support the mechanical load of the PAM, leading to the detachment of the active material from the grid (Catherino et al., 2004; Ruetschi, 2004; Yang et al., 2017).

$$2Pb + O_2 \rightarrow 2PbO \quad (4)$$

$$PbO + (n-1)O \rightarrow PbO_n \ (1 < n < 2) \quad (5)$$

$$PbO_n + (2-n)O \rightarrow PbO_2 \quad (6)$$

The phenomenon of oxygen evolution, a process that typically ensues when a cell is overcharged, offers significant insight into the degradation mechanisms of lead-acid batteries. During this process, oxygen atoms diffuse into the metallic grid and react with the Pb component, forming PbO (Pavlov, 1995; Ball et al., 2002b; Ruetschi, 2004). With sustained overcharging, the formed PbO further reacts with the evolved oxygen, forming other lead-oxide phases.

The stoichiometry of the resultant corrosion layer is determined by the relative rate of these reactions and the available oxygen concentration. Notably, the corrosion layer composition varies across the layer's thickness. It has been proposed that the region of the layer closer to the grid exhibits a nominal composition of PbO_n, where n ranges from 1 to 1.5. This nominal composition suggests a non-stoichiometric or mixed-valent state of lead oxide, which indicates a lower oxygen concentration near the metallic grid (Pavlov, 1995; Ball et al., 2002b; Ruetschi, 2004).

In stark contrast, the layer region nearer to the PAM is predominantly characterized by stoichiometric PbO_2. This observation is attributed to the higher concentrations of oxygen that occur farther from the grid, promoting the formation of PbO_2 (Pavlov, 1995; Ball et al., 2002b; Ruetschi, 2004).

In many instances, the failure of lead-acid batteries can be attributed to grid corrosion, a factor critically explored by various authors. Ball et al. conducted a comparative study of physicochemical differences between grids extracted from "good" and "bad" cells, focusing primarily on the thickness of the corrosion layers (Ball et al., 2002a). No excessive thickening was observed in the "good" cells, in contrast to the "bad" cells that exhibited significant growth of the corrosion layer. Interestingly, this exponential growth mainly occurred towards the end of the cell's life. The growth rate of the corrosion layer is influenced by the number of battery cycles and is particularly accelerated in cells with reduced capacity. While overcharging is a crucial factor in forming this layer, its thickening is also a result of cumulative damage from repeated cycling. Consequently, the thickness of the corrosion layer is not solely linked to the duration of voercharge but also to the frequency of battery cycles and the condition of the cells, with more pronounced effects in cells of diminished capacity. Notably, "bad" cells, which possess reduced capacity and are easily charged, tend to overcharge for extended periods, leading to more oxygen evolution and accelerated corrosion (Ball et al., 2002a).

Subsequent studies further emphasized the role of electrolyte concentration in grid corrosion. Lander's study discovered an increase in grid corrosion rate with decreasing H_2SO_4 concentration, indicating a relationship between electrolyte

dilution, water content, and the prevalence of different lead oxide phases in the resultant corrosion layer (Lander, 1956; Yang et al., 2017). In a similar vein, Li et al. reported improved corrosion resistance of Pb-Sn alloy grids in more concentrated H_2SO_4, with these alloys producing less oxygen during cycling (Li et al., 2011). However, the corrosion layer formed in diluted H_2SO_4 showed higher electrical conductivity (Li et al., 2011).

Additionally, the nature of the corrosion layer's PbO_2 polymorphs holds significance for battery performance. Among these, α-PbO_2, a superior electron conductor favored in less acidic environments, is preferred over β-PbO_2, given its mechanical strength and adhesive properties (Bullock and Tiedemann, 1980; Shiomi et al., 2003). High acid concentrations near the grid, resulting in a corrosion layer primarily composed of β-PbO_2, increase the likelihood of premature capacity loss (Shiomi et al., 2003).

Furthermore, processes like self-discharge at an open circuit and the creation of cracks and pores within the corrosion layer can harm battery performance (Ball et al., 2002b; Culpin and Rand, 1991; Ruetschi, 2004). When the layer's PbO thickness surpasses a critical value, the grid becomes resistive, driving further self-discharge and the formation of $PbSO_4$ crystals. These crystals can create stress-induced pores and cracks that may allow the electrolyte to react with the grid and even lead to an "interface layer effect, " significantly decreasing battery capacity (Dimitrov and Pavlov, 2001; Shiomi et al., 2003).

Given these observations, controlling the thickness of the corrosion layer emerges as a key to preserving the electrode's current-carrying capability and preventing grid degradation. Other influential factors include operational parameters like temperature and electrode potential and grid characteristics such as microstructure and composition (Lander, 1956; Bullock and Tiedemann, 1980; Shiomi et al., 2003; Li et al., 2011). Hence, understanding and mitigating grid corrosion is critical for improving lead-acid battery lifespan and performance.

The methods known about alloying to mitigate grid corrosion are provided in Section 3.2.

3 Prolonging cycle life by material-based intervention

In the preceding section, the potential mechanisms leading to battery failure were explored, explicitly focusing on irreversible sulfation affecting the negative electrode, alongside PAM degradation and grid corrosion impacting the positive electrode. The focus now shifts to a range of innovative methods devised to enhance the performance of LAB components. These strategies are conceived to counteract or delay capacity loss, thereby deferring the onset of battery failure. Understanding and addressing these critical facets of LAB longevity pave the way toward achieving more sustainable and durable energy storage solutions.

3.1 Active material expanders

3.1.1 NAM expanders

Battery failure triggered by irreversible sulfation of the NAM has led to the implementation of additives, commonly termed "expanders." One of the pioneer expanders employed to delay this irreversible sulfation was barium sulfate ($BaSO_4$). When distributed within the NAM matrix, $BaSO_4$ crystals act as alternative sites for $PbSO_4$ to crystallize (Willihnganz, 1947). This intriguing behavior was explored by Vermian et al., who embedded $BaSO_4$ particles onto the surface of a Pb electrode and examined the sulfation dynamics using atomic force microscopy and potential sweep techniques. Their findings confirmed that, due to isomorphism, $PbSO_4$ crystals preferentially grow on $BaSO_4$ seeds (Vermesan et al., 2004). Crucially, they discovered that $BaSO_4$ addition could counterbalance the overpotential required for $PbSO_4$ nucleation, although the specific concentration and particle size of $BaSO_4$ seeds remained undisclosed. Further investigation by Pavlov et al. delved into the role of $BaSO_4$ in NAM sulfation, indicating that voltammetric data from the NAM/$BaSO_4$ composite demonstrated improved reversibility of charge-discharge reactions compared to bare NAM (Figure 6) (Vermesan et al., 2004).

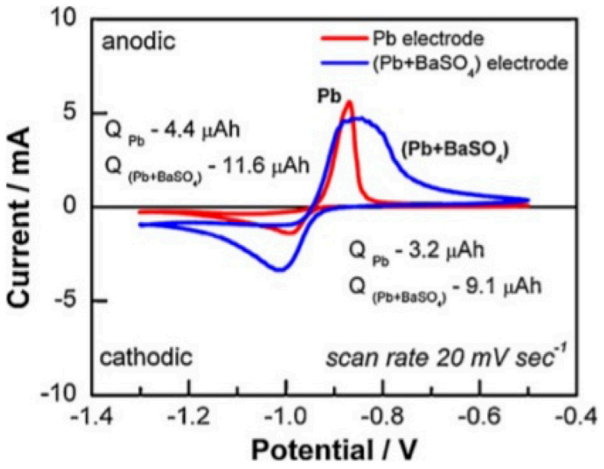

FIGURE 6
Voltammetric curves for Pb and (Pb + $BaSO_4$) electrodes immersed in H_2SO_4. A charge ratio approaching one for the (Pb + $BaSO_4$) electrode suggests enhanced reversibility of sulfation (Pavlov et al., 2010).

It was hypothesized that $BaSO_4$ nuclei attract Pb^{2+} ions during discharge, mitigating the formation of a continuous $PbSO_4$ layer; for optimal cycle life, 1.0 wt% $BaSO_4$ was advised to be added to precursor paste (Pavlov et al., 2010). Further, nano-sized $BaSO_4$ incorporated into NAM revealed a porous matrix that enhanced ionic transport compared to micron-sized $BaSO_4$ (Hosseini et al., 2019).

Moreover, lignin, a soluble polymer, improves accumulator terminal voltage and resists passivation in deep-cycle cells (Vanýsek et al., 2020). The absence of lignin, previously introduced via wooden separators, shortened cycle life due to irreversible sulfation (Pavlov, 2011). Lignin dissolved in H_2SO_4 was found to inhibit the average size increase of $PbSO_4$ crystals during the initial discharge phase, maintaining a high electrode surface area (Knehr et al., 2015).

Indulin AT, a commercial lignin product, presented mixed results when applied to NAM. It resulted in tiny $PbSO_4$ crystals enabling ion penetration but exhibiting gradual dissolution during

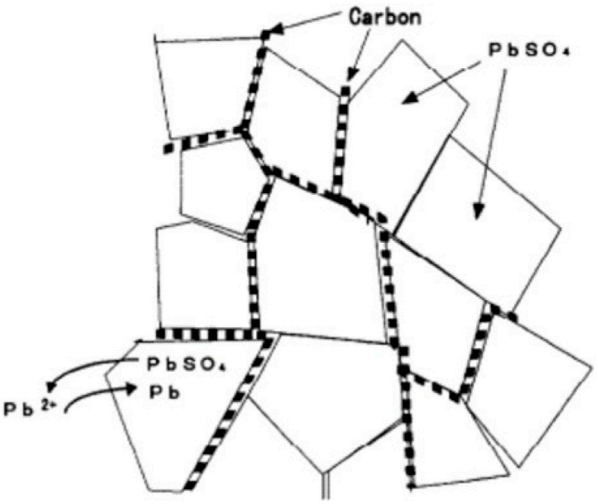

FIGURE 7
The introduction of carbon to the NAM is posited to accelerate the $PbSO_4$ reduction process by creating a conductive network that enhances charge movement (Shiomi et al., 1997).

charging (Vanýsek et al., 2020). Nevertheless, the enhanced capacity and improved NAM utilization from lignin use outweighed these drawbacks (Hirai et al., 2009; Pavlov et al., 2010).

Finally, as an additive, carbon increases discharged cell conductivity and reduces sulfation effects. It forms a conductive matrix along $PbSO_4$ crystals, enhancing the reduction rate and mitigating $PbSO_4$ accumulation, as depicted in Figure 7 (Shiomi et al., 1997; Kumar et al., 2014; Swogger et al., 2014; Yeung et al., 2015; Banerjee et al., 2016; Banerjee et al., 2017; Lach et al., 2019; Mithin Kumar et al., 2019; Yin et al., 2020; Yin et al., 2021). Research endeavors have focused on integrating carbon into NAMs to develop enhanced LABs, commonly referred to as lead-carbon batteries (LCBs). This advancement in battery technology has been comprehensively examined in existing scholarly reviews (Mahadik et al., 2023).

Yeung et al. reported a 140% performance boost in lead-acid batteries under partial state of charge (PSoC) cycling upon adding 0.2 wt% graphene to the negative active material (NAM) (Yeung et al., 2015). SEM images showed 25% smaller $PbSO_4$ crystals with improved charge mobility in Pb/graphene samples, enhancing $PbSO_4$ formation reversibility, consistent with other carbon additive studies (Shiomi et al., 1997; Kumar et al., 2014; Swogger et al., 2014; Banerjee et al., 2016; Banerjee et al., 2017; Lach et al., 2019; Mithin Kumar et al., 2019; Shen et al., 2021). In a related study, Thong et al. employed a PSoC-based methodology to evaluate the performance of carbon-coated NAMs, revealing enhanced cycle durability compared to traditional LABs (Thong et al., 2023).

Utilizing hierarchical porous carbon (HPC) with macro- (>50 nm) and meso- (2–50 nm) pores can further enhance carbon incorporation. HPC facilitates ionic transport and increases active surface area for Pb deposition and $PbSO_4$ dissolution, improving reduction onset and PSoC cycle stability (Yin et al., 2020; Shen et al., 2021). However, it was observed that carbon additives can catalyze hydrogen evolution, thus requiring measures to mitigate this effect for optimal performance (Yin et al., 2020; Shen et al., 2021).

In addition, oxygen functionalization of carbon additives could reduce NAM sulfation. Surface oxygen defects lead to homogeneous Pb nucleation on carbon, enhancing kinetics and redox reversibility and curbing hydrogen evolution rates (Yin et al., 2020; Shen et al., 2021; Yin et al., 2021). Nevertheless, the effects of carbon addition on hydrogen evolution and water loss are still debated in the literature, emphasizing the need for comprehensive measures to suppress hydrogen evolution (Yin et al., 2020; Shen et al., 2021; Yin et al., 2021).

3.1.2 PAM expanders

Due to its outstanding physical properties and resilience under highly acidic conditions, carbon has been widely exploited as a NAM expander. Particularly in the context of the positive electrode, where structural degradation is a prevalent failure mechanism, carbon additives chiefly function as structural support (Ball et al., 2003; Ponraj et al., 2009; Yang et al., 2017; Lach et al., 2019; Mandal et al., 2021). Additionally, forming interconnected pores upon carbon incorporation can foster effective electrolyte diffusion. Such channels bridge isolated PbO_2 to the grid, enhancing material utilization and conversion (Ball et al., 2003; Ponraj et al., 2009; Yang et al., 2017; Lach et al., 2019; Mandal et al., 2021).

Interestingly, incorporating 0.25 wt% carbon fiber into red-lead-based PAM resulted in a 20% capacity surge at elevated discharge rates. SEM imaging of cycled plates synthesized with carbon revealed the existence of large cavities with embedded fibers (Ball et al., 2003; Hao et al., 2018; Mandal et al., 2021). These open channels permit electrolyte accessibility to the active material that might otherwise have been forfeited due to $PbSO_4$ deposition. Remarkably, despite cyclic swelling and contraction, the porous architecture of the PAM is preserved, a testament to the support provided by the carbon fibers. The increased pore rigidity helps bolster the PAM, delaying its softening.

Furthermore, carbon enhances charge transport and distributes the charge uniformly across the current collecting grid, thereby lessening the corrosion rate by mitigating excessive load (Ball et al., 2003; Hao et al., 2018; Mandal et al., 2021). In the realm of LCBs, ongoing challenges are presented by the oxidative characteristics of the PAM, thereby highlighting the necessity for grid materials with enhanced corrosion resistance. Recent progress in this domain has been marked by incorporating carbon mesh within electrode grids, a development that has notably augmented conductivity and longevity (Mahadik et al., 2023).

Similar strengthening effects were reported for PAM synthesized with Bi additives (Lam et al., 1999). A study by Yang et al. employed the simultaneous addition of Sb_2O_3 and SnO_2 to the PAM (Lam et al., 1999; Chahmana et al., 2009; Yang et al., 2018). The inclusion of Sb_2O_3 aimed to promote the coalescence of PbO_2 (McGregor, 1996), reducing the likelihood of softening and shedding. At the same time, incorporating SnO_2 was designed to increase the hydrated zones within the PAM, thereby amplifying the electrochemical activity of the cell (Lam et al., 1999; Chahmana et al., 2009; Yang et al., 2018).

3.2 Grid alloying

Using Pb as grid material for positive electrodes has extended the lifecycle of Planté cells, but higher temperatures in modern

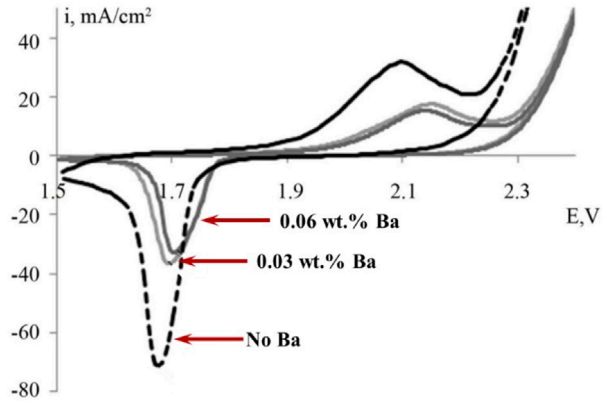

FIGURE 8
Cyclic voltammetry of positive electrodes employing Pb-Ca-Sn-Ba grids with differential Ba content. Incorporation of Ba raises the oxygen overpotential, though diminished redox currents suggest a decrease in electrochemical activity (Burashnikova et al., 2013).

VRLA batteries can expedite corrosion (Berndt and Nijhawan, 1976; Prengaman, 1995; Prengaman, 2001; Yang et al., 2017). Pb-Sb alloys offer rechargeability and stable discharge, but Sb migration can lead to water loss and premature capacity loss (Prengaman, 1995; Prengaman, 2001). Pb-Ca alloys improve mechanical properties but have limited applications due to spontaneous corrosion when in contact with PAM (Prengaman, 1995). Other elements, including Sb, Sn, and As, can potentially reduce corrosion rates (Lam et al., 1994; Prengaman, 1995; Yang et al., 2017). Incorporation of Sn into Pb-Ca systems enhances recovery from deep discharge and corrosion stability, but the brittle corrosion product may require further mechanical reinforcement (Prengaman, 2001; Rocca et al., 2006). Adding Ba into Pb-Ca-Sn increases grid hardness but reduces electrochemical activity (Burashnikova et al., 2013) (Figure 8). Further research is needed to balance these effects for optimal battery performance.

3.3 Electrolyte additives

During battery charging, side reactions such as water decomposition, leading to irreversible sulfation and grid corrosion, can occur (Pavlov et al., 2004; Yang et al., 2017; Wu et al., 2020). Mitigation strategies involve active material expanders, grid dopants, and electrolyte additives (Bullock, 1979; Yang et al., 2017). Boric acid (H_3BO_3), an additive, curtails hydrogen evolution from Pb in H_2SO_4 and enhances $PbSO_4$ conversion, although ineffective for reducing oxygen evolution (Wu et al., 2020). Higher H_3BO_3 concentrations improve PAM kinetics and lower self-discharge (Burashnikova et al., 2013). Phosphoric acid (H_3PO_4) enhances oxygen evolution overpotential and reduces PbO_2 size, aiding in extended cycle life but decreasing capacity due to fine $PbSO_4$ crystal formation (Bullock and McClelland, 1977; Bullock, 1979; Sternberg et al., 1987; Garche et al., 1991; Meissner, 1997). Sodium sulfate (Na_2SO_4) limits dendritic Pb structures and hydrogen evolution and marginally prolongs cycle life (Ferreira, 2001; Weighall, 2003; Karimi et al., 2006; Karami et al., 2010; Yu et al., 2013; Zeng et al., 2015). Organic surfactants, like sodium dodecyl sulfate (SDS), have also shown promise in reducing $PbSO_4$ concentration and extending cycle life under PSoC conditions (Francia et al., 2001; Khayat Ghavami et al., 2016). These studies underscore the need for continued research into electrolyte additives for battery performance optimization.

4 Prolonging cycle life by operation-based interventions

Aside from material-based strategies, the extension of battery cycle life can also be realized through operation-based modifications. Unlike the former, which necessitates the engineering of cell components and a deep understanding of battery chemistry, operation-based interventions can be implemented in-operando or post-battery failure. These primarily aim to defer the effects of aging mechanisms through effective battery management, acknowledging that operational parameters can contribute to the emergence of these issues (Yang et al., 2017).

Operation-based interventions often involve altering charging algorithms tailored to optimize battery performance and lifespan. Modifying charging algorithms not only regulates the state of charge (SoC), depth of discharge (DoD), and charging rate but can also potentially mitigate detrimental side reactions and processes such as corrosion, gas evolution, and sulfation (Bullock, 1979; Wu et al., 2020).

In addition to adjusting charging algorithms, desulfation methods are another critical facet of operation-based interventions. As sulfation is a significant factor causing premature capacity loss in lead-acid batteries, strategic desulfation can restore battery capacity and extend the battery life (Sternberg et al., 1987; Badawy and El-Egamy, 1995; Burashnikova et al., 2013). Various techniques, including pulse charging and applying high-voltage shocks, have been explored to promote the conversion of solid $PbSO_4$ back into its active forms, effectively reversing the sulfation process (Francia et al., 2001; Khayat Ghavami et al., 2016).

4.1 LAB charging algorithms

Desulfation, encompassing techniques designed to reverse sulfation, primarily involves modifications of typical charging algorithms, given that sulfation reversal occurs during charging. Traditional LAB charging generally employs either a constant current (CC), constant voltage (CV), or a combination of both, known as the constant current-constant voltage (CC-CV) strategy (Figure 9).

CC and CV charging are widely utilized due to their simplicity. However, CC charging is generally limited to smaller currents to avoid overheating. Furthermore, not all $PbSO_4$ is converted due to voltage restrictions, resulting in a decrease in the reactivity of the regenerated active material. On the other hand, CV charging effectively prevents excessive heating, but it lacks the convective mixing necessary to recover capacity loss due to electrolyte stratification. Both methods necessitate prolonged charging periods to recover a substantial amount of active material

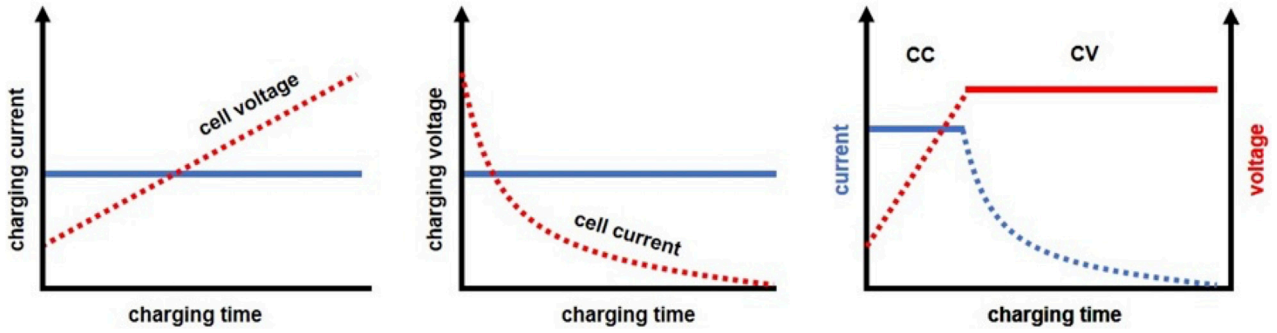

FIGURE 9
Common charging approaches for LAB: charging via constant current (left), through constant voltage (center), and by constant current-constant voltage charging method (right). The solid line illustrates the charging parameter input, whereas the dashed line signifies the subsequent cell response.

(Yamashita and Matsumaru, 1988; Hua and Lin, 2000; Catherino et al., 2004; Knehr et al., 2014; Serhan and Ahmed, 2018; Lavety et al., 2020).

A combination of CC and CV charging strategies, the CC-CV or two-step charging method, is often utilized to maximize charge acceptance and reverse sulfation from the preceding discharge. The first phase of this method involves CC charging until a preset voltage, typically ranging from 2.3 to 2.45 V per cell, is achieved. The bulk of the charge is resupplied during this phase. The second phase involves CV charging, where the cell is maintained at the preset voltage until the current reaches saturation, indicating a fully charged state. This CV phase plays a pivotal role in the CC-CV charging process, and the duration of this stage substantially affects charge acceptance. The cell should remain at the float voltage long enough to maximize active material recovery, but a balance must be struck to minimize water loss and gas evolution. Other factors influencing charge acceptance during CC-CV charging include the end-of-charge potential, charging current, length of the CV phase, and DoD (Hua and Lin, 2000; Catherino et al., 2004; Sauer et al., 2007; Kujundžić et al., 2017; Franke and Kowal, 2018; Serhan and Ahmed, 2018; Lavety et al., 2020). Despite its advantages, the CC-CV charging strategy also inherits the extensive charging periods characteristic of both CC and CV methods.

The strategy of pulsed charging has also been proposed for LAB maintenance. This approach diverges from conventional charging strategies that continuously apply charging parameters. Instead, pulsed charging employs periodic high currents with specific waveforms, as depicted in Figure 11 (left). Applying high current induces a high instantaneous voltage, which promotes rapid recovery and random nucleation of active material. The short duration of these pulses hinders excessive growth of active material, with successive pulses inducing nucleation. A relaxation period is included to facilitate internal electrolyte neutralization and double-layer overpotential dissipation (Hua and Lin, 2000; Cheung et al., 2006; James et al., 2006; Lavety et al., 2020).

Reflex charging is a variant of the pulsed charging technique and includes a negative pulse in addition to the positive pulse and relaxation interval. This waveform resembles that illustrated in Figure 11 (right). The negative pulse helps to alleviate the polarization problem common to LABs. A previous patent proposed that negative pulses contribute to forming tiny, round, active material crystals. These crystals demonstrate better chemical activity than regular crystals (Podrazhansky and Popp, 1994; Bizhani et al., 2021).

An electro-thermal model was used to compare the charging performance of CC-CV, pulsed, and reflex charging strategies on a 12 V/50 Ah LAB, and regarding charging time, pulsed and reflex charging strategies achieved 100% SoC more rapidly than CC-CV charging. Although this finding is consistent with most patent claims, it introduces the trade-off of excessive heating, which negatively impacts battery health (Burkett and Bigbee, 1971; Podrazhansky and Popp, 1989; Ookita, 1999; Dykeman, 2005; Bizhani et al., 2021). Overheating issues can often be mitigated by adjusting the pulse width of the waveform (James et al., 2006; Singh and Karandikar, 2017; Lavety et al., 2020). A study conducted by James et al. reported improved capacity in relatively new submarine-grade lead acid twin-cells that had previously failed factory acceptance tests. They developed a charging device capable of delivering adjustable positive and negative pulses, demonstrating that pulsed charging equalized and enhanced the twin cells' capacity, seemingly reducing gas evolution during subsequent charging stages. However, this technique proved less effective on older cells (4–5 years old), indicating that in some instances, sulfation becomes permanent (James et al., 2006).

Mizumoto et al. trialed a combination of on-off constant current charging and large, short discharge pulses to restore the capacity of degraded starter and deep-cycle batteries. This charging strategy is similar to reflex charging but with intermittent application of the discharge pulse. The implementation of this strategy resulted in successful capacity recovery for the starter battery, evidenced by a cold cranking ampere and discharge time comparable to those of a new unit. In contrast, a starter battery charged using conventional CV had less than half the discharge time. Employing on-off current charging increases the likelihood of returning the battery to near-new condition when the battery has not exceeded 3 years of use and has never been over-discharged to less than 10.2 V. For deep-cycle batteries, this recovery method is only effective for batteries up to 3 years old, with a maximum recovery of 80%–90% of the original discharge time (Mizumoto et al., 2018).

A technique referred to as inverse charging was also proposed, aiming to recover the capacity of electrodes that have already failed due to irreversible sulfation. This technique leverages the fact that

the reduced form of $PbSO_4$ (R-$PbSO_4$) is more electrochemically active than its oxidized form (O-$PbSO_4$). Although inverse charging is not a unique algorithm, it can act as an intermediary process before full recharge. The inverse charging scheme initially converts O-$PbSO_4$ to PbO_2, which is then reduced to form R-$PbSO_4$. Since this phase is electrochemically active, the final recharge step to recover Pb is facilitated (Karami et al., 2009; Zhang et al., 2010; Zhang et al., 2011; Spanos et al., 2016). This technique was first demonstrated by Yamamoto et al., who used a three-electrode setup and confirmed its effectiveness in reactivating passivated Pb (Yamamoto et al., 1996).

Karami et al. applied inverse charging to fully sulfated flooded batteries, showing that 80%–90% of the nominal capacity could be recovered after a full recharge, depending on the approach used for inverse charging (CC, CV, or pulsed current). Scanning electron microscope (SEM) images revealed that after inverse charging, large $PbSO_4$ crystals from both electrodes were dissolved, resulting in an increased surface area and discharge capacity. Zhang et al. and Spanos et al. corroborated the beneficial effects of inverse charging in their independent studies, with Spanos et al. observing that grid composition influenced the efficacy of the process. Positive grids containing tin (Sn) suffered significant capacity loss, presumably due to Sn dissolution and loss of active material connectivity (Karami et al., 2009; Zhang et al., 2010; Spanos et al., 2016).

4.2 LAB charging with active feedback sensing

Degradation in battery capacity is often driven by a complex interplay of aging mechanisms that can co-occur, overlap, or follow sequentially. By monitoring specific parameters during the charging process, the state of health (SoH) can be estimated, and the active aging mechanisms can be identified. The cell's response can also discern the limiting cells involved and adjust the charging parameters accordingly.

Shi et al. employed a pressure-sensing approach for desulfating and remedying a valve-regulated lead acid battery. Transducer sensors were fitted to individual cell compartments to measure voltage and gauge pressure during operation. The desulfation algorithm developed employs a pressure feedback mechanism in which the charging current is adjusted based on the internal pressure of the cell. The concept behind this strategy is to apply the maximum charging current to convert $PbSO_4$ within a tolerable pressure range that prevents water loss and gas evolution. The desulfation algorithm partially reverses capacity loss, suggesting that irreversible sulfation was not the sole aging mechanism at play. Nevertheless, the diagnostic step accurately identified irreversible sulfation as the leading cause of capacity loss (Shi et al., 2013).

Tao et al. utilized a resonance method for non-invasive sulfation diagnosis and simultaneous capacity restoration. This technique is predicated on the relationship between electric capacitance and sulfation. While battery capacitance is essentially constant, progressive sulfation will cause changes in the relative dielectric constant, altering the system's frequency response. The resonance method diagnoses the state of sulfation by measuring the resonance frequency from the break frequency and comparing this with analytical results derived from electrochemical impedance spectroscopy. This same resonance frequency is then used for subsequent restoration. In their study, Tao et al. selected three classes of batteries with differing sulfation states for restoration. The resonance method resulted in an overall decrease in capacitive impedance and a partial increase in capacity. Subsequent analysis of the samples revealed significant changes in the active material morphology, as illustrated in Figure 10. Before restoration, a dense layer of sulfation comprised of smooth and large particles occupied the surface. Application of the resonance method resulted in a reduction in particle size and the restoration of the porous structure of the active material (Tao et al., 2021).

4.3 Passive battery management

Restoration methodologies only sometimes yield successful results, mainly when irreversible sulfation is not the only aging mechanism at work. Some of the studies referenced above recovered only a fraction of the capacity despite the application of proposed techniques. Passive solutions such as a robust battery management system for appropriate charging and discharging are crucial to effectively mitigate premature battery failure and prolong cycle life (James et al., 2006; Karami et al., 2009; Zhang et al., 2010; Shi et al., 2013; Tao et al., 2021).

Singh et al. suggested a hybrid energy storage system (HESS) that consists of the LAB and an auxiliary ultracapacitor linked to a bidirectional DC-DC converter. The proposed charging control aims to balance battery temperature and charging rate. A charge controller maintains the SoC within 20% and 80%. Moreover, a power management controller modulates power flow based on the load drive cycle. The demand requirement and voltage regulation are optimized using a Fractional-Order-Proportional-Integral-Derivative algorithm. Depending on the feedback from the rule-based strategy, a pulse width modulator sends signals to the bidirectional DC-DC converter. If the battery is overcharged, the ultracapacitor stores the surplus energy. This system circumvents deep discharge and prevents peak load demand by maintaining a balance between the battery temperature and charging rate. Simulations showed that the proposed method effectively maintained constant voltage, temperature, and current output. This battery management system proficiently computes the charging and discharging profiles based on the power cost assessment of the algorithm, thus reducing the risk of water decomposition and $PbSO_4$ agglomeration (Singh et al., 2021).

Lavety et al. (2020) employed a temperature feedback mechanism to implement temperature-regulated pulsed (TRPC) and reflex charging (TRRC) strategies. In both TRPC and TRRC, a reference temperature range is used to decide the charging strategy. In TRPC, as shown in Figure 11 (left), the battery temperature, Tbat, may fall into two categories. If T_{bat} lies within the prescribed range, a constant current is supplied to charge the battery. If $T_{bat} > T_{max}$ during charging, the current is switched to zero until $T_{bat} < T_{min}$. This protocol is repeated until a preset SoC is reached; at this point, charging is switched to CV mode. For TRRC, as shown in Figure 11 (right), an additional reference point, maximum discharge temperature (T_{dis}), is provided, and T_{bat} may fall into one of three categories. Between T_{min} and T_{max}, a constant current is supplied. Current is supplied to an input capacitor between T_{max}

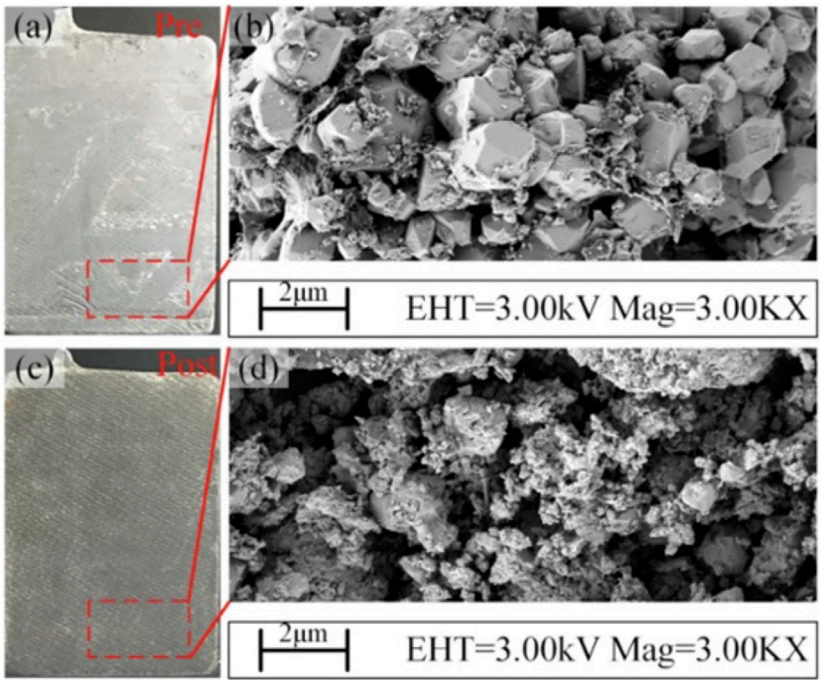

FIGURE 10
Optical **(A,C)** and SEM **(B,D)** images of a retired battery pre **(A,B)** and post **(C,D)** desulfation via the resonance method. The implementation of the resonance method led to a decrease in the particle size of the active material (Tao et al., 2021).

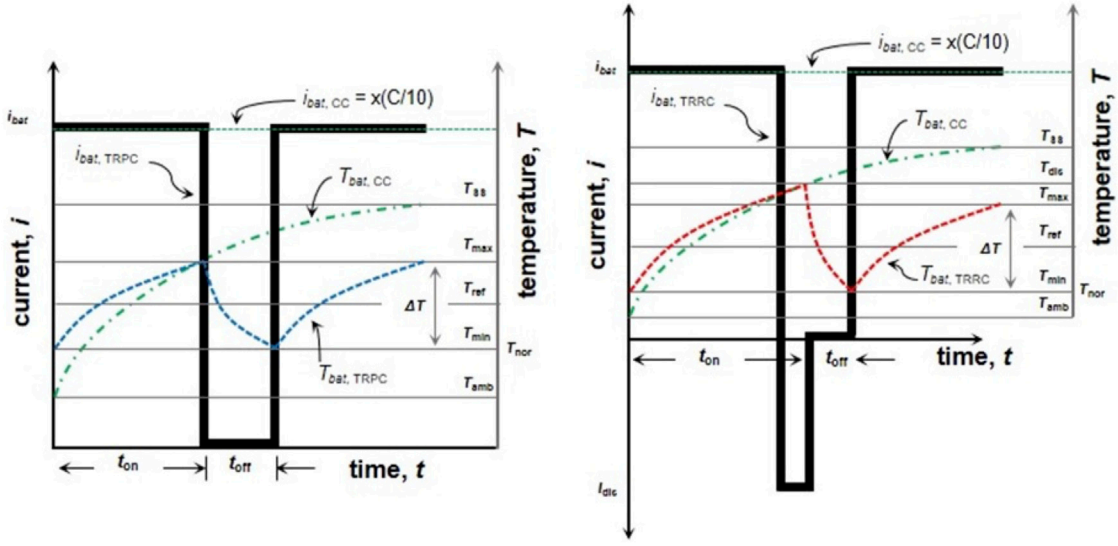

FIGURE 11
Thermal-regulated pulsed (left) and reflex (right) charging patterns. These charging schemes use the temperature of the battery to determine the input variables (Lavety et al., 2020).

and T_{dis}. Above T_{dis}, the current is switched to zero to allow the battery to cool. This cycle is repeated until the battery reaches 95% SoC (Lavety et al., 2020). As shown in Supplementary Table S1, TRPC and TRRC resulted in more charge deposition, less heating, and overall, less SoH decay compared to the reference CC-CV charging (Lavety et al., 2020).

Tomantschger proposed an air-lift pump system to mitigate electrolyte stratification, a primary factor in irreversible sulfation (Tomantschger, 1984). Air pulses were introduced via Teflon tubes to agitate the electrolyte. This strategy enhanced battery discharge energy at temperatures above 20°C and halved charging time, resulting in less water loss and gas evolution (Figure 12, left).

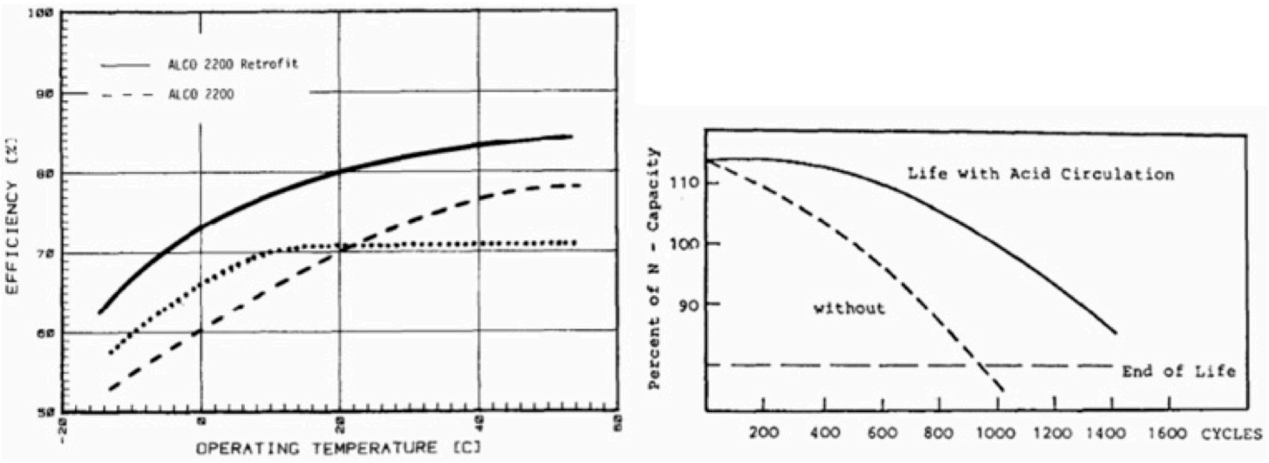

FIGURE 12
Illustration of the modified flooded-LAB design (left). The supplemental air lift pump enhances acid movement, leading to improved capacity exploitation and extended cycle lifespan (right) (Tomantschger, 1984).

However, the added energy needed for the pump decreased efficiency slightly, and the system significantly improved cycle life (Figure 12, right), highlighting the importance of innovative strategies to address complex aging mechanisms in lead-acid batteries (Tomantschger, 1984).

5 Ultrasound as a potential candidate for LAB cycle life improvement

Building on Tomantschger's research, which observed improvements in cycle life upon agitation of the battery, an alternate method of introducing vibration through sound waves has been proposed. A patent issued to Kelly and Galgana (Kelly and Galgana, 2009) suggests integrating a device capable of producing mechanical vibrations into the LAB. The concept hinges on preventing covalent bonding between the chemical reaction products and the LAB matrix by mechanical excitations. As a result, this method reportedly enhances the LAB's chemical-to-electrical energy conversion process, thereby significantly improving energy performance. However, despite its intriguing premise, this proposal needs a scientific framework to substantiate the claims.

Recently, the application of acoustic waves to prolong the cycle life has been demonstrated in Li-metal batteries (LMB). Huang et al. integrated a surface acoustic wave (SAW) device into a pouch cell sample to facilitate electrolyte streaming during charging, as shown in Figure 13A (Huang et al., 2020). Experiments involving constant current deposition revealed a more uniform voltage profile when SAW was activated, compared to a continuous voltage drop observed during Li deposition without SAW. This profile suggests that acoustic streaming fosters uniform Li deposition, a finding corroborated by subsequent imaging experiments that revealed a thin, dense, and dendrite-free layer.

Simulation results in Figures 13B, C indicate that acoustic streaming decreases Li concentration gradients in the electrolyte, promoting uniform Li deposition. A comparison of the cycle performance between control and SAW-LMB revealed similar capacity and charge retention at C-rates less than 1C. However, the performance of the control cell deteriorated significantly at C-rates above 1C, with the discrepancy becoming more apparent as the C-rate increased. The stability of the SAW-LMB was also reflected in the charge-discharge voltage profiles, with only a 10% increase in polarization voltage observed between cycles 10 and 200. This stability indicates that Li dendrite formation and 'dead' Li are less prevalent when acoustic waves are applied during charging. By promoting uniform Li deposition and inhibiting early dendritic growth, even when the cell operates near its limiting current density, SAW-driven flow significantly enhances the performance of the LMB. Overall, the improved performance of SAW-LMB can be attributed to the enhancement of Li-ion transport facilitated by acoustic streaming (Huang et al., 2020).

An essential claim made by Huang et al. is the chemistry-agnostic nature of their methodology (Huang et al., 2020), suggesting that the technique could be adapted to various battery chemistries that employ liquid electrolytes. Within the context of lead-acid systems, ultrasound or general acoustic waves have thus far been limited to characterizing the SoC or SoH (Swoboda et al., 1983; Liu and Li, 2012; Guillet et al., 2021). As of yet, only a few studies have reported on the impact of ultrasound-driven flow on the cycle life of LABs (Kasumzade, 2020; Juanico, 2022; Peng, 2022).

An electroacoustic charging method described in a patent application by Juanico (2022) resulted in a notable increase (of at least 20%) in LAB cycle life, echoing the "charge coup de fouet" (CCdF) observed in prior experiments (Delaille et al., 2006). Delaille et al. (2006) linked this phenomenon to mass transport effects, possibly due to a rise in the bisulfate ion (HSO_4^-) concentration in pores partially obstructed by PbSO4 crystals from prior discharge, rather than PbSO4 resistance as previously postulated. Notably, while CCdF was not evident during the initial charge cycle following full discharge in these experiments, the electroacoustic charging consistently exhibited CCdF-like behavior. Separate strategies presented by Kasumzade (2020) and later supported by Peng (2022) employed inertial acoustic cavitation to disrupt pore obstructions through the explosive effect of cavitation bubbles.

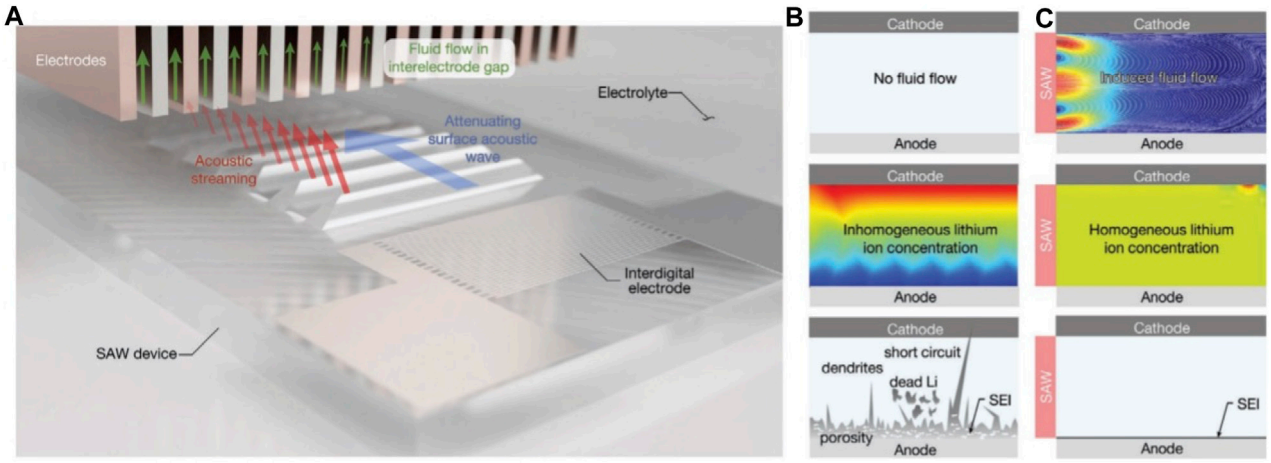

FIGURE 13
An illustrative progression of acoustic streaming's effect on LMB behavior is shown: **(A)** Suggested diagram of acoustic streaming in an LMB, facilitated by a Surface Acoustic Wave (SAW) device. **(B)** In the absence of acoustic streaming, irregular Li ion concentration occurs, leading to the formation of dendrites. **(C)** Acoustic streaming aids in maintaining a homogeneous Li ion concentration, thereby ensuring Li deposition free of dendrites (Huang et al., 2020).

The maintenance of the LAB electrode structure without degradation due to the intense pressures from such bubble bursts remains uncertain. Alternatively, electroacoustic charging uses non-inertial cavitation to adjust pore pressure distribution on electrode surfaces, facilitating HSO_4^- pore penetration, as hypothesized by Delaille et al., thereby stalling degradation from $PbSO_4$ pore blockage.

The data indicate that incorporating acoustic energy during electroacoustic charging augments the cell's capacity to uptake an electrical charge, optimizing its charge capacity (Juanico, 2022). Such augmentation may slow the cell's aging, prolonging its life cycle. Pending studies aim to explore the foundational processes governing the interplay between sound and cell electrochemistry throughout the charging phase, with a specific interest in fine-tuning sound wave delivery to cell compartments.

Promising results indicate that electroacoustic charging may serve as a viable method to extend the cycle life of lead-acid cells. This improvement can be realized without material-based methods to enhance the cell's electrochemical properties or adopting other operation techniques relying on active feedback sensing (as covered in Section 4.2). The sole prerequisite for this enhancement is additional energy input via sound. Subsequent cycling analyses revealed no overt signs of grid corrosion (Juanico, 2022), such as an eroded electrode grid or its segments (elaborated in Section 2.3).

Ultrasound appears to play a pivotal role in extending the cycle life of lead-acid cells by influencing key electrochemical processes. It is hypothesized that the application of ultrasound induces a phenomenon akin to CCdF (Delaille et al., 2006), which lowers the cell's potential for extended periods, thereby mitigating the rapid thickening of the corrosion layer. This lower potential is crucial as it slows down one of the primary degradation pathways in these cells (Ball et al., 2002a). Further, ultrasound augments electrochemical reactions within the cell, effectively delaying the onset of sulfation, a major cause of cell failure. Notably, introducing sound waves results in a controlled increase in temperature, which stays within safe limits, ensuring the integrity of the cell components. This temperature rise, likely related to the propagation of pressure waves, does not risk boiling the electrolyte or displacing active material from the electrode grid.

Moreover, these pressure waves, characterized by patterns of compression and rarefaction, seem to modify the pore pressure distribution on the electrode surfaces. As per the insights from patent application WO 2022/191721 (Juanico, 2022), this alteration enhances the permeation of electrolyte ions into the electrode matrix, increasing the likelihood of interaction with electrons from the current input. This enhanced interaction could elucidate the improvement in cell capacity utilization, leading to an extended cycle life. In essence, a process similar to sonoporation may occur on the electrode surfaces, allowing a transient yet significant influx of penetrating ions, a critical factor in the enhanced capacity utilization of the electrodes.

It can be inferred that enhancements in cycle life attributed to electroacoustic charging in individual lead-acid cells can translate to larger assemblies comprising multiple cells (Kasumzade, 2020; Juanico, 2022; Peng, 2022). This observation broadens the implications of integrating electroacoustic charging technology into LABs in expansive renewable energy storage systems. An extended cycle life in such batteries could amplify the lifespan and economic feasibility of renewable energy storage mechanisms. These preliminary insights underscore the imperative for ongoing research to confirm the scalability of benefits from electroacoustic charging in multicell LAB configurations and to evaluate the prospects for broader adoption of this technology within renewable energy storage infrastructure.

6 Outlook for LAB with electroacoustic charging

Sound-assisted battery operation can significantly enhance the cycle life of flooded LABs. This technology can be integrated straightforwardly into stationary flooded LABs (Juanico, 2022), especially in renewable energy (RE) storage applications. This assertion is validated by a techno-

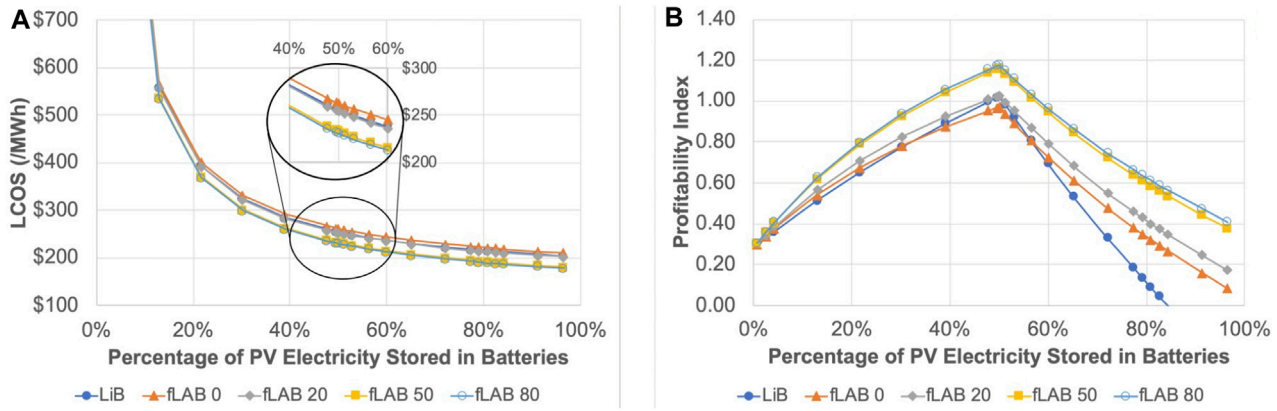

FIGURE 14
Depicting the financial impacts of improved battery longevity, the figure demonstrates: **(A)** the trend in the Levelized Cost of Storage (LCOS), and **(B)** the Profitability Index in relation to the percentage of harvested energy stored in Lithium-Ion Battery (LiB), flooded Lead-Acid Battery (fLAB), and an envisioned fLAB enhanced by 20%, 50%, and 80% in cycle life. In the accompanying legend, "fLAB 0"refers to the baseline fLAB, while "fLAB 20," "fLAB 50," and "fLAB 80," signify fLABs with cycle life improvements of 20%, 50%, and 80%, respectively.

economic analysis, considering the profitability and levelized cost of flooded LABs with extended cycle life, informed by pertinent data from existing literature. This comparison is made in a best-case scenario for lithium-ion batteries (LiBs), the most extensively deployed battery type in RE storage systems. The optimistic assumptions underpinning this analysis include a storage cost of $100/kWh (Hsieh et al., 2019), situated at the lower threshold of projections for the year 2045 (Cole et al., 2021), coupled with a recycling rate of 8% — double the prevailing average rate (Bae and Kim, 2021). These optimistic assumptions serve as a buffer in the analysis in anticipation of advancements in LiB technology research and development that will effectively reduce costs and significantly enhance recyclability before 2030. This scenario contrasts with the baseline and improved flooded LABs, showcasing varying degrees of prolonged cycle life.

The comparative evaluation hinges on two pivotal metrics: the levelized cost of storage (LCOS) and the profitability index (PI). The LCOS and PI are derived from the net present value of discounted monetary and energy values. LCOS represents the ratio of the total discounted cost to the total discounted electricity generated over the lifetime of the RE project (El Fathi and Outzourhit, 2018; Killer et al., 2020; Steckel et al., 2021). Conversely, PI embodies the revenue aspect of the project, denoting the ratio of the net present value of discounted cash flows to the initial capital investment. In this framework, revenues comprise electricity sales and carbon incentives, with the latter being defined by the value of carbon emissions from fossil fuels averted through substitution with RE. Although LCOS is a prevalent tool in evaluating the feasibility of energy projects, it offers a partial view of viability by solely focusing on the cost component. PI furnishes a broader view by additionally considering the revenue facet. Therefore, both metrics are presented to delineate the distinctions between the baseline and improved flooded LABs compared to the most optimistic LiB scenario for RE storage.

This analysis (see Supplementary Material for detailed calculations) involves a 50-MW solar PV facility that has been operational for 20 years and is expected to harness sunlight for approximately 6 h daily. This sunlight duration is typical for tropical countries, such as the Philippines. The cost model considers nighttime energy demands to be half of daily energy requirements. Any unmet demand during nighttime, not fulfilled by the battery reserves, is covered by coal-powered generation. The assumption holds that all batteries undergo replacement upon reaching their respective end of life (EOL)–dictated by the established assumptions, manifests as 8 years for LiBs (Steckel et al., 2021) and spans 5, 6, 7.5, and 9 years for baseline (Dhundhara et al., 2018), 20%, 50%, and 80%-improved flooded-LAB, respectively.

With a 95% recycling rate, the EOL recycling cost for LABs translates to $0.64/kWh, whereas for LiBs, with an 8% recycling rate, it amounts to an exorbitant $472/kWh. The target storage cost for LiBs is assumed to be $100/kWh (Hsieh et al., 2019), whereas flooded LABs are considered at the high end of their current price, $245/kWh (May et al., 2018). Each 10% increase in LAB cycle life nudges this price by an additional 1%. Despite these numbers, the EOL costs favor flooded LABs due to their high recycling rates. For simplicity, the annual operational expense is set to be $21.90/kW, regardless of battery type, a value that is consistent with literature estimates considering capacity fade (Steckel et al., 2021). This value equates to a daily operational cost of approximately $10/MWh for a storage system with a 6-h capacity operating 365 calendar days a year. The carbon benefits are applied consistently across LiBs and flooded LABs based on the latest estimates of the social cost of carbon (Hänsel et al., 2020).

Utilizing LCOS parameters from literature sources (Supplementary Table S2), a decline in LCOS (US$/MWh) is observed with increased harvested PV electricity stored in batteries, as illustrated in Figure 14A. Within the 40%–60% range of PV electricity stored in batteries, LCOS fluctuates between $200 and $300/MWh, aligning with published LCOS estimates for second-life (Steckel et al., 2021) and new LiBs (Jülch, 2016; Killer et al., 2020; Oliveira et al., 2021) as well as flooded-LABs (El Fathi and Outzourhit, 2018) in energy storage applications. The detail in Figure 14A emphasizes that a modest 20% extension of LAB cycle life could render it competitive with optimistic projections for LiBs. Moreover, an elevation to an 80% extension in LAB cycle life does not foster a substantial LCOS improvement compared to a 50% extension, indicating a phenomenon of diminishing returns.

While the decline of LCOS with increased stored electricity may appear advantageous, it can be misleading as it only considers the cost side of the equation, thus not fully justifying the investment. Battery sizing should consider the relative nighttime demand when solar PVs are not generating electricity. If nighttime demand is less than what is stored in the batteries, surplus electricity cannot be sold.

The profitability index (PI), computed with the same parameters as in Supplementary Table S2, offers more apparent differentiation among LiBs, baseline, and hypothetical improved flooded LABs than LCOS. Even when applying the same revenue parameters for both LiB and flooded-LAB (Supplementary Table S2), differences in economic viability projections are determined primarily by battery replacement and EOL recycling/disposal costs. Figure 14B illustrates the optimal battery storage capacity as 50% of PV electricity, matching the assumed nighttime energy demand. A PI less than 1.0 signifies an unprofitable endeavor, whereas PI more significant than 1.0 suggests a profitable investment, with profits increasing as PI moves further above 1.0. The optimum PI is consistently below 1.0 for baseline flooded-LAB, indicative of the ongoing issue of short cycle life, which erodes the benefits of high recyclability. Conversely, the optimum PI for LiBs is slightly above 1.0, but this assumes that the target storage cost of $100/kWh and twice higher recycling rates have been achieved.

If LAB cycle life were improved by 20%, even with a 2% premium on storage price for the additional electroacoustic-charger technology enabling this enhancement, the optimal PI would be on par with the optimistic LiB. This outcome highlights the critical role of LAB cycle life in economic considerations. Therefore, addressing the deep-cycle life issue in flooded LABs could substantially benefit their viability for RE storage. Additionally, the PI plots affirm the diminishing returns for more than 50% cycle-life enhancement shown by the LCOS comparison in Figure 14A. However, in these scenarios, the profitability appears less sensitive to the criterion of matching the percentage of energy stored with the nighttime demand.

7 Summary

The review provides an insightful overview of the lead-acid battery (LAB), a technology extensively used since the 19th century. Despite its age, LABs are highly recyclable and crucial in various applications, from large-scale energy storage in power grids to small-scale uses like vehicle starters. However, LABs face challenges like a relatively short cycle life and lead toxicity, which have shifted focus to alternative technologies like lithium-ion batteries (LiBs).

The paper identifies the main setbacks of LABs, particularly the short cycle life resulting from various aging mechanisms, such as sulfation, grid corrosion, and positive active material degradation. These factors significantly impact the battery's efficiency and longevity, prompting research into methods for extending cycle life.

The review then categorizes the strategies to address these challenges into two primary approaches: material-based and operation-based. Material-based methods focus on altering the composition of cell components to counteract aging processes, while operation-based strategies involve modifying battery operation, like charging techniques, to mitigate aging effects.

A key highlight of the review is introducing an innovative ultrasound-based technique, initially successful in lithium-metal batteries, showing promise for enhancing LAB cycle life. This method could potentially revitalize interest in LAB research.

Lastly, the paper examines the economic implications of extending LAB cycle life, particularly in renewable energy storage. Comparing LABs with LiBs suggests that even modest improvements in LAB cycle life could significantly boost their market competitiveness.

The review illuminates the enduring importance of LAB technology, outlining the challenges, recent advancements, and potential economic impacts of innovations in the field. It emphasizes the necessity for ongoing research and development to optimize and rejuvenate this longstanding battery technology.

Author contributions

DJ: Conceptualization, Formal Analysis, Funding acquisition, Resources, Writing–original draft, Writing–review and editing.

Funding

The author(s) declare financial support was received for the research, authorship, and/or publication of this article. Department of Science and Technology (DOST) Grant # 10047 and Philippine Council for Industry, Energy, and Emerging Technologies Research & Development (PCIEERD) Grant # 8337.

Acknowledgments

The author acknowledges the funding support from the DOST "Science for Change Program" under the Niche Centers for R&D in the Regions (NICER) subprogram and the PCIEERD BATTERY program. The author also recognizes the contributions of the team comprising X. Galapia, A. Ardiente, N. A. Rodelas, N. R. Pacleb, J. Biscocho, P. V. Nonat, A. Callao, N. Aguel, K. Salazar, E. Festijo and P.E. Reyes.

Conflict of interest

The author declares that the research was conducted in the absence of any commercial or financial relationships that could be construed as a potential conflict of interest.

Publisher's note

Supplementary material

The Supplementary Material for this article can be found online at: https://www.frontiersin.org/articles/10.3389/fbael.2023.1268412/full#supplementary-material

References

Archdale, G., and Harrison, J. A. (1972). The anodic dissolution of Pb in H_2SO_4. *J. Electroanal. Chem. Interfacial Electrochem.* 39 (2), 357–366. doi:10.1016/S0022-0728(72)80159-1

Badawy, W. A., and El-Egamy, S. S. (1995). Improvement of the performance of the positive electrode in the lead/acid battery by addition of boric acid. *J. Power Sources* 55 (1), 11–17. doi:10.1016/0378-7753(94)02022-U

Bae, H., and Kim, Y. (2021). Technologies of lithium recycling from waste lithium ion batteries: a review. *Mater. Adv.* 2 (10), 3234–3250. doi:10.1039/d1ma00216c

Baird, J. K., Hill, S. C., and Clunie, J. C. (1999). Kinetics of protein crystal nucleation and growth in the batch method. *J. Cryst. Growth* 196 (2-4), 220–225. doi:10.1016/S0022-0248(98)00839-2

Ball, R. J., Evans, R., Thacker, E. L., and Stevens, R. (2003). Effect of valve regulated lead/acid battery positive paste carbon fibre additive. *J. Mater. Sci.* 38, 3013–3017. doi:10.1023/A:1024727820753

Ball, R. J., Kurian, R., Evans, R., and Stevens, R. (2002a). Failure mechanisms in valve regulated lead/acid batteries for cyclic applications. *J. Power Sources* 109 (1), 189–202. doi:10.1016/S0378-7753(02)00071-X

Ball, R. J., Kurian, R., Evans, R., and Stevens, R. (2002b). Influence of positive active material type and grid alloy on corrosion layer structure and composition in the valve regulated lead/acid battery. *J. Power Sources* 111 (1), 23–38. doi:10.1016/S0378-7753(02)00221-5

Banerjee, A., Ziv, B., Levi, E., Shilina, Y., Luski, S., and Aurbach, D. (2016). Single-wall carbon nanotubes embedded in active masses for high-performance lead-acid batteries. *J. Electrochem. Soc.* 163 (8), A1518–A1526. doi:10.1149/2.0261608jes

Banerjee, A., Ziv, B., Shilina, Y., Levi, E., Luski, S., and Aurbach, D. (2017). Single-wall carbon nanotube doping in lead-acid batteries: a new horizon. *ACS Appl. Mater. Interfaces* 9 (4), 3634–3643. doi:10.1021/acsami.6b13377

Berndt, D., and Nijhawan, S. C. (1976). Lead-acid batteries with low antimony alloys. *J. Power Sources* 1 (1), 3–15. doi:10.1016/0378-7753(76)80002-X

Bizhani, H., Sani, S. K. H., Rezazadeh, H., and Muyeen, S. M. (2021). "A comprehensive comparison of a lead-acid battery electro-thermal performance considering different charging profiles," in IEEE 4th International Conference on Computing, Power and Communication Technologies (GUCON), Germany, September 24-26, 2021 (IEEE), 1–6. doi:10.1109/GUCON50781.2021.9573724

Broda, B., and Inzelt, G. (2020). Investigation of the electrochemical behaviour of lead dioxide in aqueous sulfuric acid solutions by using the *in situ* EQCM technique. *J. Solid State Electrochem.* 24, 1–10. doi:10.1007/s10008-019-04450-y

Bullock, K. R. (1979). The effect of phosphoric acid on the positive electrode in the lead-acid battery: III. Mechanism. *J. Electrochem. Soc.* 126 (11), 1848–1853. doi:10.1149/1.2128813

Bullock, K. R., and McClelland, D. H. (1977). The effect of phosphoric acid on the positive electrode in the lead acid battery. *J. Electrochem. Soc.* 124 (10), 1478–1482. doi:10.1149/1.2133095

Bullock, K. R., and Tiedemann, W. H. (1980). The corrosion of a strontium-lead alloy in sulfuric acid. *J. Electrochem. Soc.* 127 (10), 2112–2118. doi:10.1149/1.2129356

Burashnikova, M. M., Zotova, I. V., and Kazarinov, I. A. (2013). Pb-Ca-Sn-Ba grid alloys for valve-regulated lead acid batteries. doi:10.4236/eng.2013.510A002

Burkett, W. B., and Bigbee, J. H. (1971). *U.S. Patent No. 3,597,673*. Washington, DC: U.S. Patent and Trademark Office, 597. Available at: https://patentimages.storage.googleapis.com/1e/5e/fd/a478d39be30fdb/US3597673.pdf.

Catherino, H. A., Feres, F. F., and Trinidad, F. (2004). Sulfation in lead–acid batteries. *J. Power Sources* 129 (1), 113–120. doi:10.1016/j.jpowsour.2003.11.003

Chahmana, N., Matrakova, M., Zerroual, L., and Pavlov, D. (2009). Influence of some metal ions on the structure and properties of doped β-PbO_2. *J. Power Sources* 191 (1), 51–57. doi:10.1016/J.JPOWSOUR.2008.11.066

Chang, T. G. (1984). Structural changes of positive active material in lead-acid batteries in deep-discharge cycling. *J. Electrochem. Soc.* 131 (8), 1755–1762. doi:10.1149/1.2115955

Cheung, T. K., Cheng, K. W. E., Chan, H. L., Ho, Y. L., Chung, H. S., and Tai, K. P. (2006). "Maintenance techniques for rechargeable battery using pulse charging," in 2nd International Conference on Power Electronics Systems and Applications, USA, 12-14 Nov. 2006 (IEEE), 205–208. doi:10.1109/PESA.2006.343100

Cole, W., Frazier, A. W., and Augustine, C. (2021). Cost projections for utility-scale battery storage: 2021 update *(No. NREL/TP-6A20-79236)*. Golden, CO (United States): National Renewable Energy Lab.NREL. doi:10.2172/1786976

Culpin, B., and Rand, D. A. J. (1991). Failure modes of lead/acid batteries. *J. Power Sources* 36 (4), 415–438. doi:10.1016/0378-7753(91)80069-A

D alkaine, C. V., Mengarda, P., and Impinnisi, P. R. (2009). Discharge mechanisms and electrochemical impedance spectroscopy measurements of single negative and positive lead-acid battery plates. *J. Power Sources* 191 (1), 28–35. doi:10.1016/j.jpowsour.2008.12.097

Delaille, A., Perrin, M., Huet, F., and Hernout, L. (2006). Study of the "coup de fouet" of lead-acid cells as a function of their state-of-charge and state-of-health. *J. Power Sources* 158 (2), 1019–1028. doi:10.1016/j.jpowsour.2005.11.015

Dhundhara, S., Verma, Y. P., and Williams, A. (2018). Techno-economic analysis of the lithium-ion and lead-acid battery in microgrid systems. *Energy Convers. Manag.* 177, 122–142. doi:10.1016/J.ENCONMAN.2018.09.030

Dimitrov, M., and Pavlov, D. (2001). Influence of grid alloy and fast charge on battery cycle life and structure of the positive active mass of lead acid batteries. *J. Power Sources* 93 (1-2), 234–257. doi:10.1016/S0378-7753(00)00598-X

Dykeman, S. W. (2005). *U.S. Patent No. 6,841,974*. Washington, DC: U.S. Patent and Trademark Office, 841. Available at: https://patentimages.storage.googleapis.com/07/0c/a3/ade0355a172d4a/US6841974.pdf.

Egan, D. R. P., Low, C. T. J., and Walsh, F. C. (2011). Electrodeposited nanostructured lead dioxide as a thin film electrode for a lightweight lead-acid battery. *J. Power Sources* 196 (13), 5725–5730. doi:10.1016/J.JPOWSOUR.2011.01.008

El Fathi, A., and Outzourhit, A. (2018). Technico-economic assessment of a lead-acid battery bank for standalone photovoltaic power plant. *J. Energy Storage* 19, 185–191. doi:10.1016/J.EST.2018.07.019

Ferreira, A. L. (2001). Battery additives: any influence on separator behavior? *J. Power Sources* 95 (1-2), 255–263. doi:10.1016/S0378-7753(00)00622-4

Francia, C., Maja, M., and Spinelli, P. (2001). Electrochemical characterisation of expander materials. *J. Power Sources* 95 (1-2), 119–124. doi:10.1016/S0378-7753(00)00612-1

Franke, M., and Kowal, J. (2018). Empirical sulfation model for valve-regulated lead-acid batteries under cycling operation. *J. Power Sources* 380, 76–82. doi:10.1016/j.jpowsour.2018.01.053

Gandhi, K. S. (2020). Modeling of sulfation in a flooded lead-acid battery and prediction of its cycle life. *J. Electrochem. Soc.* 167, 013538–13541. doi:10.1149/1945-7111/ab679b

Garche, J., Döring, H., and Wiesener, K. (1991). Influence of phosphoric acid on both the electrochemistry and the operating behaviour of the lead/acid system. *J. Power Sources* 33 (1-4), 213–220. doi:10.1016/0378-7753(91)85060-A

Guillet, N., Gau, V., and Kirchev, A. (2021).Ultrasonic interrogation of AGM-VRLA batteries, LABAT'21-11th International Conference on Lead-Acid Batteries, 26th–28th January 2024, China. IEEE. Available at: https://hal-cea.archives-ouvertes.fr/cea-03215022.

Guo, Y., Yan, W., and Hu, J. (2007). Effects of electrolyte stratification on performances of flood lead-acid batteries. *J. Electrochem. Soc.* 154 (1), A1. doi:10.1149/1.2364807

Hänsel, M. C., Drupp, M. A., Johansson, D. J., Nesje, F., Azar, C., Freeman, M. C., et al. (2020). Climate economics support for the UN climate targets. *Nat. Clim. Change* 10 (8), 781–789. doi:10.1038/s41558-020-0833-x

Hao, H., Chen, K., Liu, H., Wang, H., Liu, J., Yang, K., et al. (2018). A review of the positive electrode additives in lead-acid batteries. *Int. J. Electrochem. Sci.* 13 (3), 2329–2340. doi:10.20964/2018.03.70

Hirai, N., Kubo, S., and Magara, K. (2009). Combined cyclic voltammetry and *in situ* electrochemical atomic force microscopy on lead electrode in sulfuric acid solution with or without lignosulfonate. *J. Power sources* 191 (1), 97–102. doi:10.1016/j.jpowsour.2008.10.090

Hossain, M. D., Islam, M. M., Hossain, M. J., Yasmin, S., Shingho, S. R., Ananna, N. A., et al. (2020). Effects of additives on the morphology and stability of PbO_2 films electrodeposited on nickel substrate for light weight lead-acid battery application. *J. Energy Storage* 27, 101108. doi:10.1016/J.EST.2019.101108

Hosseini, S., Farhadi, K., and Banisaeid, S. (2019). Improving particle size of BaSO4 with a unique glycerol base method and its impact on the negative active material of the lead-acid battery. *J. Energy Storage* 21, 139–148. doi:10.1016/j.est.2018.11.003

Hsieh, I. Y. L., Pan, M. S., Chiang, Y. M., and Green, W. H. (2019). Learning only buys you so much: practical limits on battery price reduction. *Appl. Energy* 239, 218–224. doi:10.1016/J.APENERGY.2019.01.138

Hua, C. C., and Lin, M. Y. (2000). A study of charging control of lead-acid battery for electric vehicles. In ISIE'2000. Proceedings of the 2000 IEEE International Symposium on Industrial Electronics (Cat. No. 00TH8543) 4-8 Dec. 2000,USA , (Vol. 1, pp. 135–140). IEEE. doi:10.1109/ISIE.2000.930500

Huang, A., Liu, H., Manor, O., Liu, P., and Friend, J. (2020). Enabling rapid charging lithium metal batteries via surface acoustic wave-driven electrolyte flow. *Adv. Mater.* 32 (14), 1907516. doi:10.1002/adma.201907516

Hutchinson, R. (2004). *Temperature effects on sealed lead acid batteries and charging techniques to prolong cycle life (No. SAND2004-3149)*. Albuquerque, NM, and Livermore, CA (United States): Sandia National Laboratories SNL. doi:10.2172/975252

James, M., Grummett, J., Rowan, M., and Newman, J. (2006). Application of pulse charging techniques to submarine lead-acid batteries. *J. Power Sources* 162 (2), 878–883. doi:10.1016/j.jpowsour.2005.02.018

Jin, J. E., Jin, D., Shim, J., and Shim, W. (2017). Enhancing reversible sulfation of PbO2 nanoparticles for extended lifetime in lead-acid batteries. *J. Electrochem. Soc.* 164 (7), A1628–A1634. doi:10.1149/2.1291707jes

Juanico, D. E. (2022). World intellectual property organization. *PCT Appl. WO*. Available at: https://patentimages.storage.googleapis.com/22/1d/82/9e59c0e00fe9df/WO2022191721A4.pdf.

Jülch, V. (2016). Comparison of electricity storage options using levelized cost of storage (LCOS) method. *Appl. Energy* 183, 1594–1606. doi:10.1016/J.APENERGY.2016.08.165

Kanamura, K., and Takehara, Z. I. (1992). Microscopic reaction site model for cathodic reduction of lead sulfate to lead. *J. Electrochem. Soc.* 139 (2), 345–351. doi:10.1149/1.2069218

Karami, H., Masoomi, B., and Asadi, R. (2009). Recovery of discarded sulfated lead-acid batteries by inverse charge. *Energy Convers. Manag.* 50 (4), 893–898. doi:10.1016/j.enconman.2009.01.010

Karami, H., Yaghoobi, A., and Ramazani, A. (2010). Sodium sulfate effects on the electrochemical behaviors of nanostructured lead dioxide and commercial positive plates of lead-acid batteries. *Int. J. Electrochem. Sci.* 5 (7), 1046–1059. doi:10.1016/S1452-3981(23)15343-0

Karimi, M. A., Karami, H., and Mahdipour, M. (2006). Sodium sulfate as an efficient additive of negative paste for lead-acid batteries. *J. Power Sources* 160 (2), 1414–1419. doi:10.1016/J.JPOWSOUR.2006.03.036

Kasumzade, F. (2020). *U. S. Pat. Appl.* (Washington, DC: U.S. Patent and Trademark Office). Available at: https://patentimages.storage.googleapis.com/e2/f3/79/7ecac510e8c9fb/US20200136198A1.pdf.

Kebede, A. A., Coosemans, T., Messagie, M., Jemal, T., Behabtu, H. A., Van Mierlo, J., et al. (2021). Techno-economic analysis of lithium-ion and lead-acid batteries in stationary energy storage application. *J. Energy Storage* 40, 102748. doi:10.1016/J.EST.2021.102748

Kelly, S. P., and Galgana, J. R. (2009). *U.S. Patent No. 7,592,094*. Washington, DC: U.S. Patent and Trademark Office. Available at: https://patentimages.storage.googleapis.com/ef/a3/12/f697fb291b8efc/US20100021798A1.pdf.

Khayat Ghavami, R., Kameli, F., Shirojan, A., and Azizi, A. (2016). Effects of surfactants on sulfation of negative active material in lead acid battery under PSOC condition. *J. Energy Storage* 7, 121–130. doi:10.1016/j.est.2016.06.002

Killer, M., Farrokhseresht, M., and Paterakis, N. G. (2020). Implementation of large-scale Li-ion battery energy storage systems within the EMEA region. *Appl. Energy* 260, 114166. doi:10.1016/J.APENERGY.2019.114166

Kim, D. K., Yoneoka, S., Banatwala, A. Z., Kim, Y. T., and Nam, K. Y. (2018). *Handbook on battery energy storage system*. Manila, Philippines: Asian Development Bank. doi:10.22617/TCS189791-2

Knehr, K. W., Eng, C., Chen-Wiegart, Y. C. K., Wang, J., and West, A. C. (2014). *In situ* transmission X-ray microscopy of the lead sulfate film formation on lead in sulfuric acid. *J. Electrochem. Soc.* 162 (3), A255–A261. doi:10.1149/2.0141503jes

Knehr, K. W., Eng, C., Wang, J., and West, A. C. (2015). Transmission X-ray microscopy of the galvanostatic growth of lead sulfate on lead: impact of lignosulfonate. *Electrochimica Acta* 168, 346–355. doi:10.1016/J.ELECTACTA.2015.04.022

Kujundžić, G., Ileš, Š., Matuško, J., and Vašak, M. (2017). Optimal charging of valve-regulated lead-acid batteries based on model predictive control. *Appl. Energy* 187, 189–202. doi:10.1016/J.APENERGY.2016.10.139

Kumar, S. M., Ambalavanan, S., and Mayavan, S. (2014). Effect of graphene and carbon nanotubes on the negative active materials of lead acid batteries operating under high-rate partial-state-of-charge operation. *RSC Adv.* 4 (69), 36517–36521. doi:10.1039/C4RA06920J

Lach, J., Wróbel, K., Wróbel, J., Podsadni, P., and Czerwiński, A. (2019). Applications of carbon in lead-acid batteries: a review. *J. Solid State Electrochem.* 23, 693–705. doi:10.1007/s10008-018-04174-5

Lam, L. T., Douglas, J. D., Pillig, R., and Rand, D. A. J. (1994). Minor elements in lead materials used for lead/acid batteries 1. Hydrogen-and oxygen-gassing characteristics. *J. Power Sources* 48 (1-2), 219–232. doi:10.1016/0378-7753(94)80018-9

Lam, L. T., Haigh, N. P., Lim, O. V., Rand, D. A. J., and Manders, J. E. (1999). Capacity and cycle-life of batteries using bismuth-bearing oxide. *J. Power Sources* 78 (1-2), 139–146. doi:10.1016/S0378-7753(99)00023-3

Lander, J. J. (1956). Further studies on the anodic corrosion of lead in H_2SO_4 solutions. *J. Electrochem. Soc.* 103 (1), 1. doi:10.1149/1.2430227

Lavety, S., Keshri, R. K., and Chaudhari, M. A. (2020). Evaluation of charging strategies for valve regulated lead-acid battery. *IEEE Access* 8, 164747–164761. doi:10.1109/ACCESS.2020.3022235

Li, D. G., Chen, D. R., Wang, J. D., and Chen, H. S. (2011). Influences of temperature, H2SO4 concentration and Sn content on corrosion behaviors of PbSn alloy in sulfuric acid solution. *J. Power Sources* 196 (20), 8789–8801. doi:10.1016/J.JPOWSOUR.2011.06.082

Liu, J., and Li, G. (2012). Frequency and temperature characteristics of an ultrasonic method for measuring the specific gravity of lead-acid battery electrolyte. *Jpn. J. Appl. Phys.* 51 (2R), 026601. doi:10.1143/JJAP.51.026601

Lopes, P. P., and Stamenkovic, V. R. (2020). Past, present, and future of lead–acid batteries. *Science* 369 (6506), 923–924. doi:10.1126/science.abd3352

Mahadik, S., Surendran, S., Kim, J. Y., Lee, D., Park, J., Kim, T., et al. (2023). Recent progress in the development of carbon-based materials in lead-carbon batteries. *Carbon Neutralization* 2 (4), 510–524. doi:10.1002/cnl2.78

Mandal, S., Thangarasu, S., Thong, P. T., Kim, S. C., Shim, J. Y., and Jung, H. Y. (2021). Positive electrode active material development opportunities through carbon addition in the lead-acid batteries: a recent progress. *J. Power Sources* 485, 229336. doi:10.1016/J.JPOWSOUR.2020.229336

Matteson, S., and Williams, E. (2015). Residual learning rates in lead-acid batteries: effects on emerging technologies. *Energy Policy* 85, 71–79. doi:10.1016/J.ENPOL.2015.05.014

May, G. J., Davidson, A., and Monahov, B. (2018). Lead batteries for utility energy storage: a review. *J. Energy Storage* 15, 145–157. doi:10.1016/J.EST.2017.11.008

McGregor, K. (1996). Active-material additives for high-rate lead/acid batteries: have there been any positive advances? *J. Power Sources* 59 (1-2), 31–43. doi:10.1016/0378-7753(95)02298-8

Meissner, E. (1997). Phosphoric acid as an electrolyte additive for lead/acid batteries in electric-vehicle applications. *J. Power Sources* 67 (1-2), 135–150. doi:10.1016/s0378-7753(97)02506-8

Mithin Kumar, S., Arun, S., and Mayavan, S. (2019). Effect of carbon nanotubes with varying dimensions and properties on the performance of lead acid batteries operating under high rate partial state of charge conditions. *J. Energy Storage* 24, 100806. doi:10.1016/j.est.2019.100806

Mizumoto, I., Yoshii, Y., Yamamoto, K., and Oguma, H. (2018). Lead-acid storage battery recovery system using on–off constant current charge and short–large discharge pulses. *Electron. Lett.* 54 (12), 777–779. doi:10.1049/el.2018.1079

Oliveira, D. Q., Saavedra, O. R., Santos-Pereira, K., Pereira, J. D., Cosme, D. S., Veras, L. S., et al. (2021). A critical review of energy storage technologies for microgrids. *Energy Syst.*, 1–30. doi:10.1007/S12667-021-00464-6

Ookita, H. (1999). *U.S. Patent No. 5,905,364*. Washington, DC: U.S. Patent and Trademark Office, 364. Available at: https://patentimages.storage.googleapis.com/cd/8c/e5/d09ba3016167d7/US5905364.pdf.

Pavlov, D. (1992). Influence of crystal and gel zones on the capacity of the lead dioxide active mass (extended abstract). *J. Power Sources* 40 (1-2), 169–173. doi:10.1016/0378-7753(92)80049-H

Pavlov, D. (1995). A theory of the grid/positive active-mass (PAM) interface and possible methods to improve PAM utilization and cycle life of lead/acid batteries. *J. Power Sources* 53 (1), 9–21. doi:10.1016/0378-7753(94)02152-S

Pavlov, D. (2011). *Lead-acid batteries: science and technology*. Germany: Elsevier.

Pavlov, D., Balkanov, I., Halachev, T., and Rachev, P. (1989). Hydration and amorphization of active mass PbO2 particles and their influence on the electrical properties of the lead-acid battery positive plate. *J. Electrochem. Soc.* 136 (11), 3189–3197. doi:10.1149/1.2096424

Pavlov, D., and Bashtavelova, E. (1986). Structural properties of the PbO2 active mass determining its capacity and the "breathing" of the positive plate during cycling. *J. Electrochem. Soc.* 133 (2), 241–248. doi:10.1149/1.2108555

Pavlov, D., Kirchev, A., Stoycheva, M., and Monahov, B. (2004). Influence of H_2SO_4 concentration on the mechanism of the processes and on the electrochemical activity of the $Pb/PbO_2/PbSO_4$ electrode. *J. Power Sources* 137 (2), 288–308. doi:10.1016/j.jpowsour.2004.06.006

Pavlov, D., Nikolov, P., and Rogachev, T. (2010). Influence of expander components on the processes at the negative plates of lead-acid cells on high-rate partial-state-of-charge cycling. Part I: effect of lignosulfonates and $BaSO_4$ on the processes of charge and discharge of negative plates. *J. Power Sources* 195 (14), 4435–4443. doi:10.1016/j.jpowsour.2009.11.060

Pavlov, D., and Pashmakova, I. (1987). Influence of the size of $PbSO_4$ crystals on their solubility and the significance of this process in the lead-acid battery. *J. Appl. Electrochem.* 17, 1075–1082. doi:10.1007/BF01024373

Peng, Z. (2022). *U.S. Patent Appl.* (Washington, DC: U.S. Patent and Trademark Office). Available at: https://patentimages.storage.googleapis.com/85/6b/20/7eeba94f36c89b/US20220246996A1.pdf.

Podrazhansky, Y., and Popp, P. W. (1989). *U.S. Patent No. 4,829,225*. Washington, DC: U.S. Patent and Trademark Office, 829. Available at: https://patentimages.storage.googleapis.com/16/8f/56/beb0ec51218d6d/US4829225.pdf.

Podrazhansky, Y., and Popp, P. W. (1994). *U.S. Patent No. 5,307,000*. Washington, DC: U.S. Patent and Trademark Office. Available at: https://patentimages.storage.googleapis.com/1c/bd/8b/95fe4d00994917/US5307000.pdf.

Ponraj, R., McAllister, S. D., Cheng, I. F., and Edwards, D. B. (2009). Investigation on electronically conductive additives to improve positive active material utilization in lead-acid batteries. *J. Power Sources* 189 (2), 1199–1203. doi:10.1016/J.JPOWSOUR.2008.12.077

Prengaman, R. D. (1995). Wrought lead-calcium-tin alloys for tubular lead/acid battery grids. *J. Power Sources* 53 (2), 207–214. doi:10.1016/0378-7753(94)01975-2

Prengaman, R. D. (2001). Challenges from corrosion-resistant grid alloys in lead acid battery manufacturing. *J. Power Sources* 95 (1-2), 224–233. doi:10.1016/S0378-7753(00)00620-0

Rand, D. A., and Moseley, P. T. (2015). "Energy storage with lead–acid batteries," in *Electrochemical energy storage for renewable sources and grid balancing* (China: Elsevier), 201–222. doi:10.1016/B978-0-444-62616-5.00013-9

Rocca, E., Bourguignon, G., and Steinmetz, J. (2006). Corrosion management of PbCaSn alloys in lead-acid batteries: effect of composition, metallographic state and voltage conditions. *J. Power Sources* 161 (1), 666–675. doi:10.1016/J.JPOWSOUR.2006.04.140

Ruetschi, P. (2004). Aging mechanisms and service life of lead–acid batteries. *J. power sources* 127 (1-2), 33–44. doi:10.1016/J.JPOWSOUR.2003.09.052

Rydh, C. J. (1999). Environmental assessment of vanadium redox and lead-acid batteries for stationary energy storage. *J. Power Sources* 80 (1-2), 21–29. doi:10.1016/S0378-7753(98)00249-3

Sauer, D. U., Karden, E., Fricke, B., Blanke, H., Thele, M., Bohlen, O., et al. (2007). Charging performance of automotive batteries—an underestimated factor influencing lifetime and reliable battery operation. *J. Power Sources* 168 (1), 22–30. doi:10.1016/J.JPOWSOUR.2006.11.064

Serhan, H. A., and Ahmed, E. M. (2018). "Effect of the different charging techniques on battery life-time," in International Conference on Innovative Trends in Computer Engineering (ITCE), USA, 19-21 Feb. 2018 (IEEE), 421–426. doi:10.1109/ITCE.2018.8316661

Shen, C., Feng, C., Zhang, N., Yang, B., Su, L., and Wang, L. (2021). Hierarchical porous carbon material regenerated from natural bamboo-leaf: how to improve the performance of lead-carbon batteries? *J. Power Sources* 516, 230664. doi:10.1016/J.JPOWSOUR.2021.230664

Shi, Y., Ferone, C. A., and Rahn, C. D. (2013). Identification and remediation of sulfation in lead-acid batteries using cell voltage and pressure sensing. *J. Power Sources* 221, 177–185. doi:10.1016/j.jpowsour.2012.08.013

Shiomi, M., Funato, T., Nakamura, K., Takahashi, K., and Tsubota, M. (1997). Effects of carbon in negative plates on cycle-life performance of valve-regulated lead/acid batteries. *J. Power Sources* 64 (1-2), 147–152. doi:10.1016/S0378-7753(96)02515-3

Shiomi, M., Okada, Y., Tsuboi, Y., Osumi, S., and Tsubota, M. (2003). Study of PCL mechanism: influence of grid/PAM state on PCL. *J. Power Sources* 113 (2), 271–276. doi:10.1016/S0378-7753(02)00522-0

Singh, A., and Karandikar, P. B. (2017). A broad review on desulfation of lead-acid battery for electric hybrid vehicle. *Microsyst. Technol.* 23, 2263–2273. doi:10.1007/s00542-016-3030-0

Singh, A., Karandikar, P. B., and Kulkarni, N. R. (2021). Mitigation of sulfation in lead acid battery towards life time extension using ultra capacitor in hybrid electric vehicle. *J. Energy Storage* 34, 102219. doi:10.1016/J.EST.2020.102219

Spanos, C., Berlinger, S. A., Jayan, A., and West, A. C. (2016). Inverse charging techniques for sulfation reversal in flooded lead-acid batteries. *J. Electrochem. Soc.* 163 (8), A1612–A1618. doi:10.1149/2.0761608jes

Steckel, T., Kendall, A., and Ambrose, H. (2021). Applying levelized cost of storage methodology to utility-scale second-life lithium-ion battery energy storage systems. *Appl. Energy* 300, 117309. doi:10.1016/J.APENERGY.2021.117309

Sternberg, S., Mateescu, A., Branzoi, V., and Apăteanu, L. (1987). Effect of H_3PO_4 on the $PbSO_4/PbO_2$ electrode in H_2SO_4 solutions. *Electrochimica Acta* 32 (2), 349–351. doi:10.1016/0013-4686(87)85047-8

Swoboda, C. A., Fredrickson, D., Gabelnick, S., Cannon, P., Hornstra, F., Yao, N., et al. (1983). Development of an ultrasonic technique to measure specific gravity in lead-acid battery electrolyte. *IEEE Trans. Sonics Ultrasonics* 30 (2), 69–77. doi:10.1109/T-SU.1983.31389

Swogger, S. W., Everill, P., Dubey, D. P., and Sugumaran, N. (2014). Discrete carbon nanotubes increase lead acid battery charge acceptance and performance. *J. Power Sources* 261, 55–63. doi:10.1016/J.JPOWSOUR.2014.03.049

Takamatsu, D., Hirano, T., Yoneyama, A., Kimura, T., Harada, M., Terada, M., et al. (2020). In operando visualization of electrolyte stratification dynamics in lead-acid battery using phase-contrast X-ray imaging. *Chem. Commun.* 56 (66), 9553–9556. doi:10.1039/d0cc03592k

Takehara, Z., and Kanamura, K. (1984). Effect on cathodic reduction of β-PbO_2 in sulfuric acid solution of surface concentration of Pb^{2+} ions formed on β-PbO_2. *Electrochimica Acta* 29 (12), 1643–1648. doi:10.1016/0013-4686(84)89004-0

Takehara, Z. I. (2000). Dissolution and precipitation reactions of lead sulfate in positive and negative electrodes in lead acid battery. *J. Power Sources* 85 (1), 29–37. doi:10.1016/S0378-7753(99)00378-X

Tao, S., Fan, H., Lei, Y., Xu, X., Sun, Y., You, B., et al. (2021). The proactive maintenance for the irreversible sulfation in lead-based energy storage systems with a novel resonance method. *J. Energy Storage* 42, 103093. doi:10.1016/j.est.2021.103093

Thong, P. T., Kim, Y. A., Lim, H., Sim, U., Seo, H., Jung, S., et al. (2023). Lead-carbon batteries for automotive applications: analyzing negative plate performance under partial state-of-charge cycles. *J. Energy Storage* 73, 109041. doi:10.1016/J.EST.2023.109041

Tomantschger, K. (1984). Effects of electrolyte agitation on the performance of lead—acid traction batteries at various temperatures. *J. Power Sources* 13 (2), 137–149. doi:10.1016/0378-7753(84)87084-6

Vanýsek, P., Bača, P., Zimáková, J., Vaculík, S., and Bouška, M. (2020). *In-situ* AFM observations of the effect of addition of glass fibers and lignosulfonates on performance of the negative active mass of a lead-acid storage battery. *J. Energy Storage* 29, 101318. doi:10.1016/J.EST.2020.101318

Vermesan, H., Hirai, N., Shiota, M., and Tanaka, T. (2004). Effect of barium sulfate and strontium sulfate on charging and discharging of the negative electrode in a lead–acid battery. *J. Power Sources* 133 (1), 52–58. doi:10.1016/J.JPOWSOUR.2003.11.071

Weighall, M. J. (2003). Techniques for jar formation of valve-regulated lead–acid batteries. *J. Power Sources* 116 (1-2), 219–231. doi:10.1016/S0378-7753(02)00706-1

Weininger, J. L. (1974). Solution-precipitation mechanism in lead-acid cell electrode reactions. *J. Electrochem. Soc.* 121 (11), 1454. doi:10.1149/1.2401707

Willihnganz, E. (1947). Storage battery addition agents. *Trans. Electrochem. Soc.* 92 (1), 281. doi:10.1149/1.3071820

Wu, Z., Liu, Y., Deng, C., Zhao, H., Zhao, R., and Chen, H. (2020). The critical role of boric acid as electrolyte additive on the electrochemical performance of lead-acid battery. *J. Energy Storage* 27, 101076. doi:10.1016/j.est.2019.101076

Yamaguchi, Y., Shiota, M., Nakayama, Y., Hirai, N., and Hara, S. (2000). *In situ* analysis of electrochemical reactions at a lead surface in sulfuric acid solution. *J. Power Sources* 85 (1), 22–28. doi:10.1016/S0378-7753(99)00377-8

Yamamoto, Y., Matsuoka, M., Kimoto, M., Uemura, M., and Iwakura, C. (1996). Potentiodynamic reactivation of a passivated lead negative electrode in sulphuric acid solution. *Electrochimica Acta* 41 (3), 439–444. doi:10.1016/0013-4686(95)00317-7

Yamashita, J., and Matsumaru, Y. (1988). Studies on the microstructure of the positive lead-acid battery plate and its electrochemical reactivity. *J. Appl. Electrochem.* 18 (4), 595–600. doi:10.1007/BF01022256

Yang, J., Hu, C., Wang, H., Yang, K., Liu, J. B., and Yan, H. (2017). Review on the research of failure modes and mechanism for lead–acid batteries. *Int. J. Energy Res.* 41 (3), 336–352. doi:10.1002/er.3613

Yang, S., Li, R., Cai, X., Xue, K., Yang, B., Hu, X., et al. (2018). Enhanced cycle performance and lifetime estimation of lead-acid batteries. *New J. Chem.* 42 (11), 8900–8904. doi:10.1039/C8NJ00542G

Yeung, K. K., Zhang, X., Kwok, S. C., Ciucci, F., and Yuen, M. M. (2015). Enhanced cycle life of lead-acid battery using graphene as a sulfation suppression additive in negative active material. *RSC Adv.* 5 (87), 71314–71321. doi:10.1039/c5ra11114e

Yin, J., Lin, N., Lin, Z., Wang, Y., Chen, C., Shi, J., et al. (2020). Hierarchical porous carbon@ PbO_{1-x} composite for high-performance lead-carbon battery towards renewable energy storage. *Energy* 193, 116675. doi:10.1016/J.ENERGY.2019.116675

Yin, J., Zhang, W., Sun, G., Xiao, S., and Lin, H. (2021). Oxygen-functionalized defect engineering of carbon additives enable lead-carbon batteries with high cycling stability. *J. Energy Storage* 43, 103205. doi:10.1016/J.EST.2021.103205

Yu, J. Y., Qian, Z. H., Zhao, M., Wang, Y. J., and Niu, L. (2013). Effects of sodium sulfate as electrolyte additive on electrochemical performance of lead electrode. *Chem. Res. Chin. Univ.* 29, 374–378. doi:10.1007/S40242-013-2261-1

Zeng, Y., Hu, J., Ye, W., Zhao, W., Zhou, G., and Guo, Y. (2015). Investigation of lead dendrite growth in the formation of valve-regulated lead-acid batteries for electric bicycle applications. *J. Power Sources* 286, 182–192. doi:10.1016/J.JPOWSOUR.2015.03.139

Zhang, B., Zhong, J., Li, W., Dai, Z., Zhang, B., and Cheng, Z. (2010). Transformation of inert $PbSO_4$ deposit on the negative electrode of a lead-acid battery into its active state. *J. Power Sources* 195 (13), 4338–4343. doi:10.1016/j.jpowsour.2010.01.038

Zhang, B., Zhong, J., Zhang, B., and Cheng, Z. (2011). Mechanism of formation of anodic excursion peaks on lead electrode in sulfuric acid. *J. Power Sources* 196 (13), 5719–5724. doi:10.1016/j.jpowsour.2011.02.045

Zhang, W. L., Yin, J., Lin, Z. Q., Shi, J., Wang, C., Liu, D. B., et al. (2017). Lead-carbon electrode designed for renewable energy storage with superior performance in partial state of charge operation. *J. Power Sources* 342, 183–191. doi:10.1016/J.JPOWSOUR.2016.12.061

Zhang, Y., Zhou, C. G., Yang, J., Xue, S. C., Gao, H. L., Yan, X. H., et al. (2022). Advances and challenges in improvement of the electrochemical performance for lead-acid batteries: a comprehensive review. *J. Power Sources* 520, 230800. doi:10.1016/J.JPOWSOUR.2021.230800